AD-A204 742

Martin Marietta Laboratories

MARTIN MARIETTA

DTIC FILE COPY

MML TR 89- 12c

4

Evolution of the Chemistry of Passive Films of Sputter-Deposited, Supersaturated Al Alloys

Annual Report
Period:
July 1, 1987 - November 30, 1988

DTIC
S ELECTE
FEB 2 2 1989
D
D CB

Prepared for:
Office of Naval Research
800 North Quincy Street
Arlington, Virginia 22217-5000
Under Contract No. N00014-85-C-0638

Submitted By:
G.D. Davis, W.C. Moshier, T.L. Fritz, and G.O. Cote
Martin Marietta Laboratories
1450 South Rolling Road
Baltimore, Maryland 21227-3898

DISTRIBUTION STATEMENT A
Approved for public release;
Distribution Unlimited

and

G.G. Long and D.R. Black
National Institute for Standards and Technology
Gaithersburg, Maryland 20899

January 1989

89 2 22 070

Unclassified

SECURITY CLASSIFICATION OF THIS PAGE

ADA 204742

REPORT DOCUMENTATION PAGE

Form Approved OMB No. 0704-0188

1a. REPORT SECURITY CLASSIFICATION: Unclassified	1b. RESTRICTIVE MARKINGS: None
2a. SECURITY CLASSIFICATION AUTHORITY	3. DISTRIBUTION/AVAILABILITY OF REPORT: Unlimited
2b. DECLASSIFICATION/DOWNGRADING SCHEDULE: None	
4. PERFORMING ORGANIZATION REPORT NUMBER(S): MML TR 89-12c	5. MONITORING ORGANIZATION REPORT NUMBER(S)
6a. NAME OF PERFORMING ORGANIZATION: Martin Marietta Corporation, Martin Marietta Laboratories; 6b. OFFICE SYMBOL (If applicable): MML	7a. NAME OF MONITORING ORGANIZATION: Defense Contract Administration Serving Management Area - Baltimore
6c. ADDRESS (City, State, and ZIP Code): 1450 S. Rolling Road, Baltimore, MD 21227- 3898	7b. ADDRESS (City, State, and ZIP Code): 300 East Joppa Road, Baltimore, MD 21204-2099
8a. NAME OF FUNDING/SPONSORING ORGANIZATION: Office of Naval Research; 8b. OFFICE SYMBOL (If applicable)	9. PROCUREMENT INSTRUMENT IDENTIFICATION NUMBER: N00014-85-C-0638
8c. ADDRESS (City, State, and ZIP Code): 800 N. Quincy Street, Arlington, VA 22217-5000	10. SOURCE OF FUNDING NUMBERS: PROGRAM ELEMENT NO. / PROJECT NO. / TASK NO. / WORK UNIT ACCESSION NO.

11. TITLE (Include Security Classification)

Evolution of the Chemistry of Passive Films of Sputter-Deposited, Supersaturated Al Alloys

12. PERSONAL AUTHOR(S)

G.D. Davis, W.C. Moshier, T.L. Fritz and G.O. Cote, G.C. Long and D.R. Black

13a. TYPE OF REPORT	13b. TIME COVERED	14. DATE OF REPORT (Year, Month, Day)	15. PAGE COUNT
Annual	FROM 7/1/87 TO 11/30/88	January 1989	

16. SUPPLEMENTARY NOTATION

17. COSATI CODES			18. SUBJECT TERMS (Continue on reverse if necessary and identify by block number)
FIELD	GROUP	SUB-GROUP	Approved for public release, distribution unlimited. Reproduction in while or in part is permitted for any purpose of the United States Government.

19. ABSTRACT (Continue on reverse if necessary and identify by block number)

Aluminum and conventional aluminum alloys are readily susceptible to localized attack in chloride-containing environments. Recently, under funding from the Office of Naval Research (contract N00014-85-C-0638), we have investigated the passivity and corrosion behavior of several super-saturated aluminum alloys formed by co-sputter deposition. In this report, we show that several of these alloys exhibit superior resistance to localized attack in electrochemical polarization measurements and salt-fog tests. X-ray photoelectron spectroscopy was used to examine the surface chemistry of the passive film as a function of applied potential for Al, Al-Ta, and Al-Zr alloys. We find that the passive film that forms on each alloy becomes enriched in oxidized solute as the specimen is anodically polarized. In general, the oxidized solute protects the substrate by restricting the ingress of chloride and oxygen and thereby preventing or reducing localized attack and film growth, respectively. Of the solutes examined to date, Ta is the most effective in this regard; the passive film on Al-Ta alloys remains thin and protective at the most noble potentials. Breakdown occurs only as the potential drop across the film becomes great enough to allow the transport of chlorides.

20. DISTRIBUTION/AVAILABILITY OF ABSTRACT	21. ABSTRACT SECURITY CLASSIFICATION
☒ UNCLASSIFIED/UNLIMITED ☐ SAME AS RPT. ☐ DTIC USERS	Unclassified
22a. NAME OF RESPONSIBLE INDIVIDUAL: Guy D. Davis	22b. TELEPHONE (Include Area Code): 301-247-0700 ext. 2376; 22c. OFFICE SYMBOL

DD Form 1473, JUN 86 — Previous editions are obsolete. — SECURITY CLASSIFICATION OF THIS PAGE

(1)

→ Tantalum, Zirconium. (typo)

Table of Contents

DTIC COPY INSPECTED 6

Accesion For
NTIS CRA&I
DTIC TAB
Unannounced
Justification
By
Distribution /
Availability Codes
Dist | Avail and / or Special
A-1

LIST OF FIGURES

EXECUTIVE SUMMARY

Aluminum and conventional aluminum alloys are readily susceptible to localized attack in chloride-containing environments. Recently, under funding from the Office of Naval Research (contract N00014-85-C-0638), we have investigated the passivity and corrosion behavior of several super-saturated aluminum alloys formed by co-sputter deposition. In this report, we show that several of these alloys exhibit superior resistance to localized attack in electrochemical polarization measurements and salt-fog tests. X-ray photoelectron spectroscopy was used to examine the surface chemistry of the passive film as a function of applied potential for Al, Al-Ta and Al-Zr alloys. We find that the passive film that forms on each alloy becomes enriched in oxidized solute as the specimen is anodically polarized. In general, the oxidized solute protects the substrate by restricting the ingress of chloride and oxygen and thereby preventing or reducing localized attack and film growth, respectively. Of the solutes examined to date, Ta is the most effective in this regard; the passive film on Al-Ta alloys remains thin and protective at the most noble potentials. Breakdown occurs only as the potential drop across the film becomes great enough to allow the transport of chorides.

I. INTRODUCTION

Aluminum and its alloys are susceptible to localized attack or pitting, especially in aqueous chloride-containing environments. The formation of pits is caused by the breakdown of the passive film resulting from its interaction with the chloride anion. The reaction forms a more soluble, and therefore less protective, film that eventually leads to the rapid localized dissolution of the metal and the formation of a pit.

This localized corrosion can be reduced through the use of inhibitors, such as chromates or molybdates, in the electrolyte.[1-4] These anionic inhibitors react with the metal to form a passive film that is resistant to attack. The elemental form of these inhibitors (Cr or Mo, for example) alternatively has been incorporated as a solute in Fe alloys and other metals to help form a protective passive film and improve the alloy's corrosion behavior. Traditionally, this has not been done with Al alloys because of their low solid solubility. Instead of providing protection, the solutes precipitate and can promote localized attack. However, supersaturated alloys have recently been formed using either RF-magnetron sputter deposition[5-8] or ion implantation.[9-12]

Aluminum alloys containing elevated levels of several refractory metals exhibit excellent resistance to pitting attack. We examined Al-Mo and Al-Cr alloys using potentiodynamic polarization and salt fog tests to study their passivity and corrosion behavior; x-ray diffraction (XRD), selected area diffraction (SAD), high resolution scanning electron microscopy (HSEM), and transmission electron microscopy (TEM) to characterize their microstructure; and x-ray photoelectron spectroscopy (XPS) to determine the chemistry of their passive films.[5-7] We found that alloys with solute concentrations up to 16 at.% Mo (Al-16Mo) and 15 at.% Cr (Al-15Cr) are metastable at room temperature. The breakdown potential, E_b for the Al-Mo alloys is significantly higher than that of pure Al and continues to increase with increasing Mo concentration, with the Mo inhibiting pit nucleation. Conversely, although E_b for the Al-Cr alloys is also greater than that of the base metal, it is relatively independent of Cr concentration within the range 2-15 at.%. The surface analysis revealed that Al is preferentially oxidized in the passive films, but that both Mo and Cr are present in the film in up to three chemical states. Corresponding to the change in Eb, the amount of Mo in the passive film increases with solute concentration whereas the amount of Cr is not strongly dependent on alloy composition. In Al-Mo alloys, the nucleation of the pits is inhibited by the presence of a molybdate layer in the passive film that

restricts the movement of Cl- anions to the alloy. For the Al-Cr alloys, pit initiation is inhibited by a CrOOH barrier layer.

In this report on the third year of this investigation, we examine the corrosion behavior of Al, Al-Mo, Al-Cr, Al-Ta, Al-Zr, Al-Cu, and Al-Si in both aerated and deaerated KCl solutions and under salt-fog and high-humidity. We then examine in detail the evolution of the passive film of Al and Al-Zr and Al-Ta alloys from the open-circuit potential, E_{oc}, to E_b in deaerated KCl and Na_2SO_4 (Al and Al-Ta only). We also report initial results in the study of the structure of the passive film on Al-Mo alloys using reflection-extended x-ray absorption fine-structure spectroscopy (reflEXAFS).

II. EXPERIMENTAL PROCEDURE

Thin alloy films were grown by RF-magnetron sputter deposition as described in detail elsewhere.[5-8] Briefly, films (approximately 1 μm thick) containing Al and either Mo, Cr, Ta, Zr, Cu, or Si were deposited onto 2-in.-dia., single-crystal substrates of polished Si. The wafers were then cleaved into sections for use in the various experiments. The composition of the alloy films was determined by dissolving the film off the Si and measuring the concentration of the elements in solution; the concentration of any contaminant (e.g., C and O) was below the XPS detectability limit during sputter-depth profiling.

The sectioned specimens were prepared for electrochemical experiments by mounting them onto stainless steel holders and coating the specimen and the holder with lacquer, leaving an area of approximately 1 cm^2 exposed to the solution. After the lacquer had dried for 24 h, the specimens were immersed in the electrolyte (0.1 M KCl adjusted to pH 8 using dilute KOH or HCl), which was mechanically stirred, degassed, and purged with high-purity nitrogen. Other specimens were immersed in either aerated 0.1 M KCl at pH 7 or deaerated 0.1 M Na_2SO_4 adjusted to pH 8 with dilute H_2SO_4 or NaOH. After the rate of change in E_{oc} had dropped below 6 mV/h, the specimens were polarized anodically at 0.2 mV/s starting at E_{oc} using a Princeton Applied Research (PAR) Model 273 potentiostat. The electrochemical cell contained a Pt mesh counter-electrode with a surface area at least 10 times greater than the working electrode. The potentials were referenced to an external saturated calomel electrode (SCE).

The chemistry of passive film was investigated with a series of polarization experiments conducted using Al, Al-Ta, and Al-Zr alloys in deaerated KCl, and Al and Al-Ta in deaerated Na_2SO_4. The procedure consisted of linearly polarizing the specimens from E_{oc} to a set potential (multiples of 200 mV above E_{oc} until E_b), removing them from the electrolyte, rinsing the surfaces with high-purity water and then drying them with nitrogen, removing the lacquer, and transferring them through air into the XPS spectrometer. Approximately 4 min elapsed between polarization and insertion into the introduction chamber of the spectrometer. After examination by XPS, the specimens were once again mounted and coated with lacquer, immersed in a fresh solution, allowed to come to equilibrium, polarized to the next potential (200 mV higher than that of the previous experiment), and re-examined by XPS. This procedure of repolarizing the same specimen eliminated compositional variations between specimens and facilitated the study of changes in the passive-film chemistry as a function of applied potential. As we show below, the

specimens returned to the same E_{oc} (within a certain scatter) with each reimmersion, indicating that this approach did not cause any irreversible changes. Two specimens were used in each experiment unless otherwise stated; the quantitative data presented represent averages. Changes in the surface chemistry induced by the transfer procedure and by exposure to ultrahigh vacuum have been examined in detail.[7,13,14] Possible experimental artifacts were shown to be either small, (e.g., additional oxidation) or tractable (e.g., adventitious contamination), and the differences in the measured surface chemistry were shown to occur in the electrolyte.

The XPS measurements were made using a Surface Science Instruments Model SSX 100-03 spectrometer with monochromatized Al Ka X-ray source and a hemispherical electron energy analyzer with multichannel detection. The X-ray source was focussed to a spot size of 600 μm and the surface charge was neutralized with low-energy electrons. Binding energies were normalized to that of adventitious hydrocarbons at 284.6 eV. Survey spectra provided a qualitative analysis of the surface, whereas high-resolution spectra [with a full width at half maximum (FWHM) of the Au $4f_{7/2}$ peak of 1.1 eV] of the O 1s, C 1s, Al 2p, Ta 4f, and Zr 3d photoelectron peaks were used for quantitative analysis and chemical state determination. Quantitative analysis was obtained using peak areas and sensitivity factors determined from standards with our spectrometer. Chemical state separation was achieved by curve fitting, the details of which are presented in ref. 7. The Ta 4f and Zr 3d spin-orbit-split components were constrained with energy separations of 1.9 and 2.4 eV, respectively, and area ratios of 4:3 and 3:2, respectively.

Several salt fog and humidity tests were performed to establish the resistance of the alloys to attack in these environments. Salt fog tests were conducted according to ASTM B117-85 "Standard Method of Salt Spray (Fog) Testing" using a Singleton model 20 corrosion cabinet. The tests were conducted at a temperature of 35°C. A 5 wt.% sodium chloride solution was used to produce the fog. The humidity tests were performed in a Blue M Vapor-Temp chamber held at 65°C and 80% relative humidity. The degree of attack in both tests was determined visually; hence they are qualitative evaluations.

Three Al-Mo alloys (Al-6Mo, Al-9Mo, and Al-13Mo) were used in the reflEXAFS experiments. They were polarized to -400 mV (SCE) in 0.1 M KCl at pH 7 using the standard procedure and placed in a dessicator until they were analyzed several days later. A witness specimen for each alloy was examined by XPS and compared to the reflEXAFS specimens following the experiment, but no changes were observed as a result of the longer storage time.

The reflEXAFS measurements were performed on the U-15 beamline at the National Synchrotron Light Source (NSLS) at Brookhaven National Laboratory. The instrumentation and data analysis are described in detail elsewhere.[15] Briefly, the beamline is equipped with a toroidal grating monochromator, a gold mirror to direct the beam, and an aluminum contamination barrier to separate the experimental chamber from the storage ring. The soft x-ray beam impinges first on a phospher-coated gold mesh and then, at glancing (0.50 - 3.50°) incidence, onto the specimen (Fig. 1). The reflected beam from the specimen and the beam from the gold mesh are measured by photomultiplier tubes. The normalized intensity as a function of energy is currently being analyzed at the National Institute for Standards and Technology (NIST). A description of the analysis is given in the appendix.

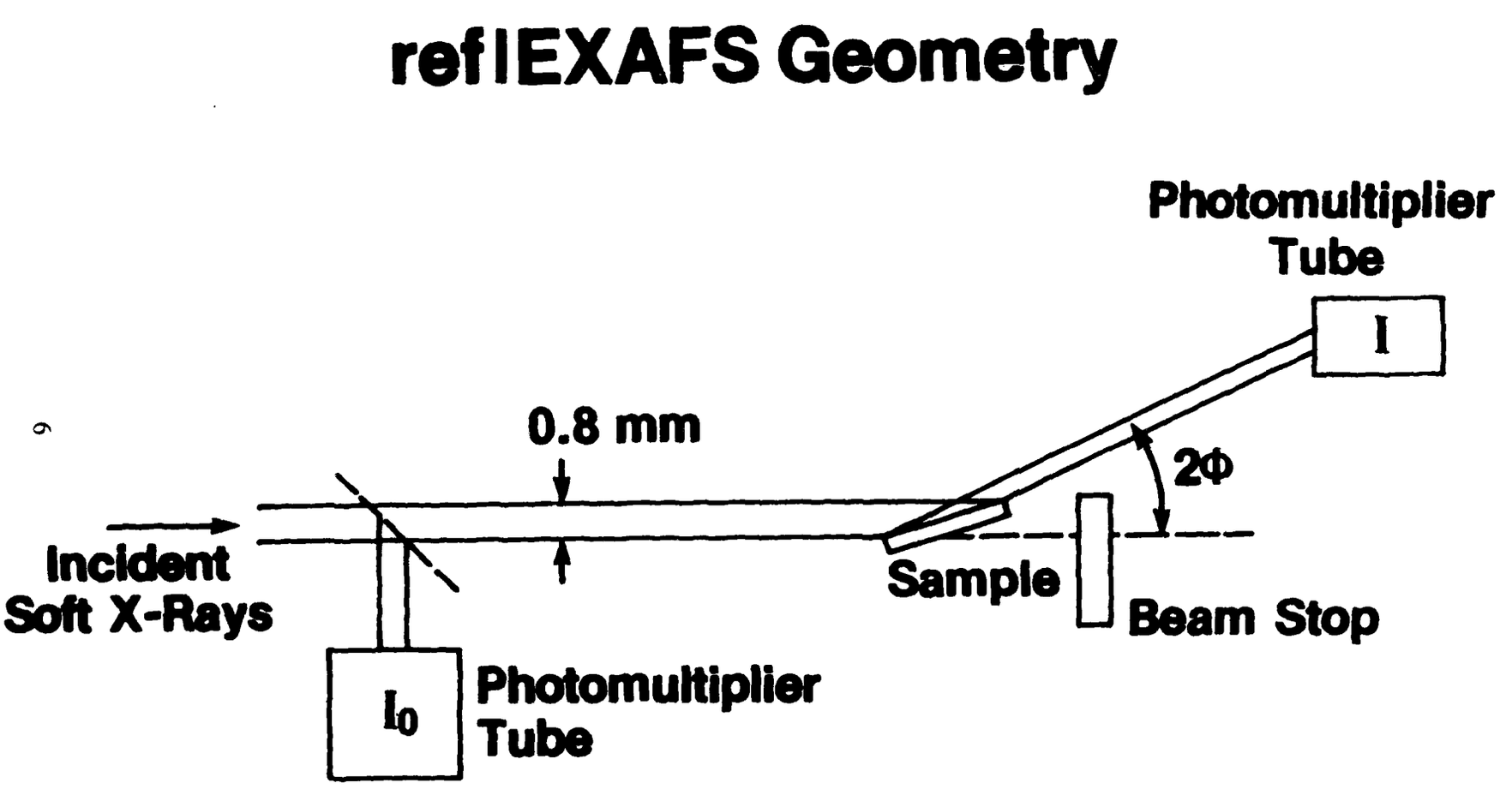

Figure 1. Experimental geometry of the reflEXAFS experiment.

III. RESULTS

A. POLARIZATION BEHAVIOR

The polarization behavior for each of the alloys in deaerated KCl is shown in Fig. 2 and that in aerated KCl is shown in Fig. 3. Each curve in the figures represents a composite of three scans performed on different specimens of each alloy. Although the power applied to the solute and Al targets during sputter deposition were the same for each alloy, the concentrations vary considerably: pure Al, Al-4Cr, Al-15Cu, Al-6Mo, Al-1Si, Al-6Ta, and Al-4Zr for the deaerated solution and pure Al, Al-4Cr, Al-19Cu, Al-8Mo, Al-1Si, Al-8Ta, and Al-3Zr for the aerated solution.

Compared to pure Al, the addition of Si and Zr had little effect on E_{oc} in the deaerated solutions, whereas E_{oc} shifted approximately 300 mV more noble with Ta and Cr, and 600 mV higher with Cu and Mo. The largest shift in E_b, to over 0 mV (SCE), was observed for the Al-Ta alloy. Progressively smaller shifts in E_b were observed for Al-Mo, Al-Cr, Al-Zr, and Al-Cu alloys and no appreciable shift was seen with Si additions.

In the air-saturated solutions, the pure Al and the Al-Cu alloy spontaneously pit; the other alloys passivated during anodic polarization prior to pitting. This passive region is smallest for Al-Si, which shifts the E_{oc} approximately 250 mV relative to pure Al but has little effect (~ 100 mV) on E_b. Al-Mo and Al-Zr alloys exhibit passive behavior over a larger potential range, with Mo increasing E_b and Zr decreasing E_{oc}, relative to pure Al. The largest passive regions are those formed with Ta and Cr additions. They lower E_{oc} by approximately 600 mV and raise E_b by a similar amount. The slight differences in the passive current densities for the Al-Mo, Al-Ta, and Al-Zr alloys noted for the two tests are probably caused by small differences in composition.

B. SALT FOG AND HUMIDITY TESTS

In the salt fog tests, Al-Ta, Al-Cr, Al-Mo, and Al-Zr specimens performed well and retained their mirror finish (although with some isolated spots or cloudy areas) after three days of exposure. In contrast, Al and the Al-Si alloy were severely attacked in these tests and were completely removed from the Si surface after three days of exposure. Longer exposure tests with the Al-Mo and Al-Cr alloys showed that the Al-Mo specimens began to discolor after 7 days.

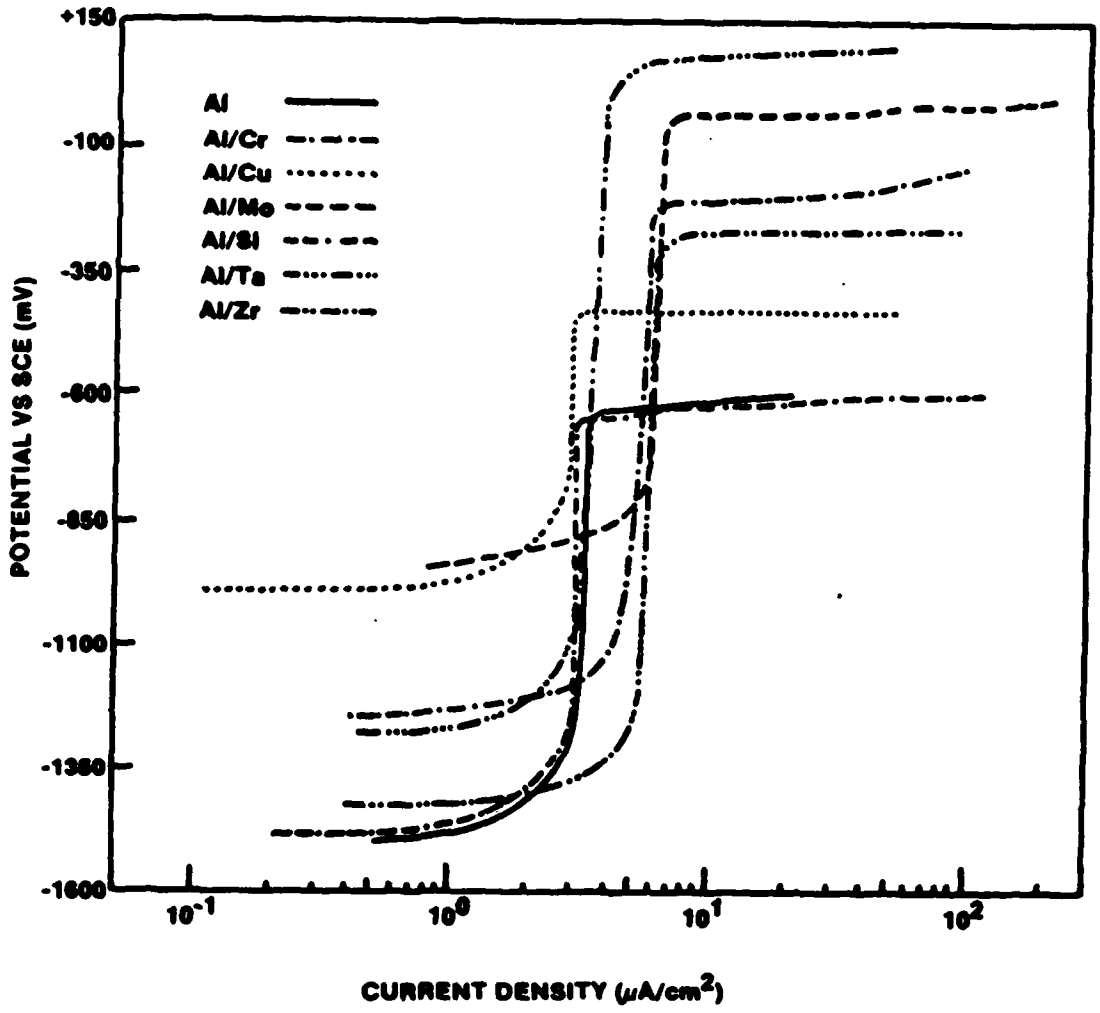

Figure 2. Potentiodynamic polarization curves for pure Al and sputter-deposited Al alloys in deaerated 0.1 M KCl at pH 8.

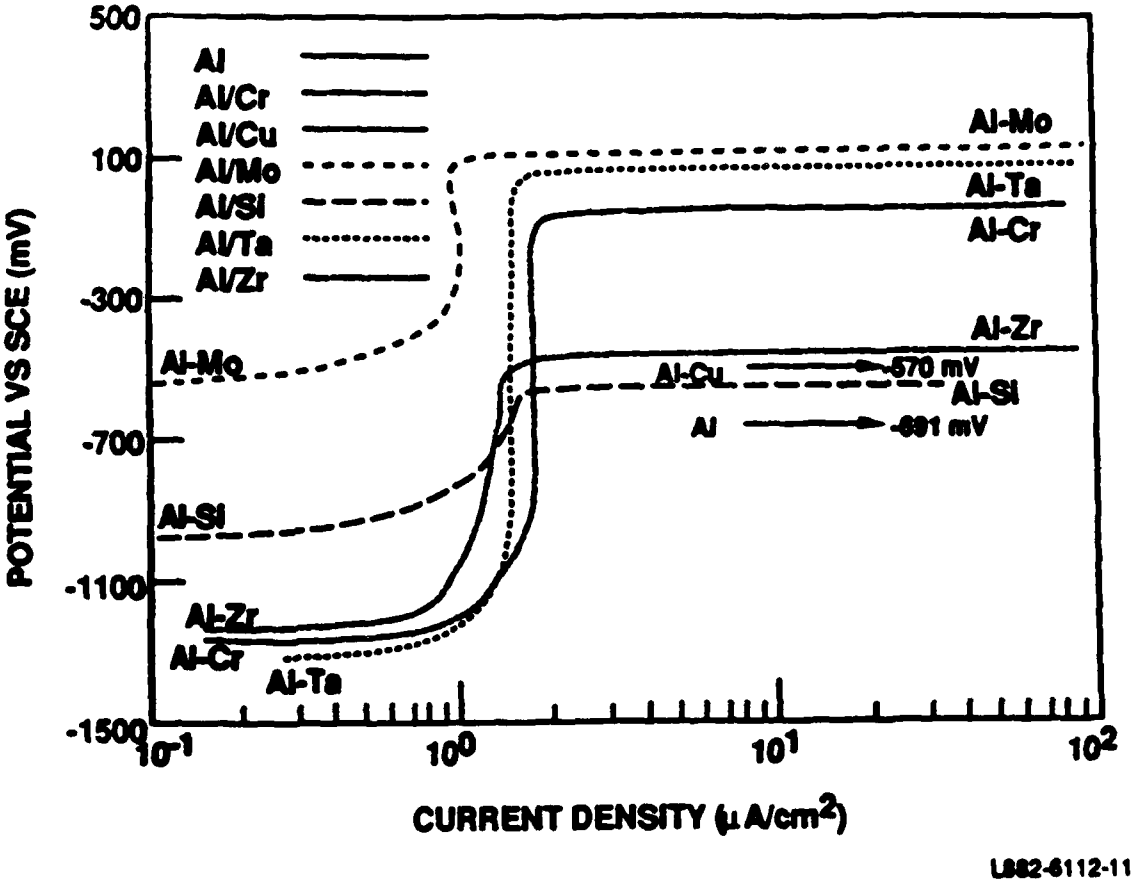

Figure 3. Potentiodynamic polarization curves for pure Al and sputter-deposited Al alloys in aerated 0.1 M KCl at pH 7.

whereas the the best Al-Cr specimens (those with low concentrations of Cr) retained their mirror finish over most of their surfaces.

Tests were conducted to determine the need to retain the solute in solution. In these tests, specimens were heated to 400°C under vacuum for 1 h prior to salt fog tests. In each case, x-ray diffraction (XRD) indicated that the solute had precipitated during aging. These specimens did not perform as well, with only the Al-Ta alloy retaining its luster after three days of exposure. Unlike the homogeneous metastable alloys, the intermetallic phases that formed during aging (with the possible exception of Al_3Ta) degraded the alloys' corrosion performance.

In contrast to the beneficial effect of the solutes in the salt fog tests, the alloys exhibited little improvement in our humidity tests compared with the hydration susceptibility of pure Al. None of the specimens consistently retained their mirror finish over the majority of their surfaces after 3 to 10 days of exposure to high humidity and temperature; instead, each surface was extensively discolored. In an attempt to improve the hydration resistance of these alloys, the specimens were treated with a hydration inhibitor prior to humidity exposure. Such hydration inhibitors have proved to be very effective in slowing the hydration of conventional Al alloys.[16-20] Alloy and pure-Al surfaces coated with either of two silane hydration inhibitors [M8500 (3 mercaptopropyltrimethoxysilane) and P810 (n- propyltrimethoxysilane)] remained shiny after 3 days, with only occasional evidence of hydration, indicating that such treatments will protect these alloys as they do pure Al and conventional Al alloys.

C. PASSIVE FILM CHEMISTRY

Based on the results presented above, we then examined in detail the evolution of the passive-film chemistry for Al-Ta and Al-Zr alloys and for Al in KCl and in Na_2SO_4 (except for Al-Zr). These alloys exhibited the best corrosion behavior among those studied. (Previously, we had performed similar studies with Al- Mo and Al-Cr.[5-7]) We will discuss elemental Al first and then present the results for the two alloys.

1. Al

The polarization experiments with the pure Al specimens are summarized in Table I. Except for the last run of specimen 1, each specimen equilibrated at approximately the same potential at the beginning of each run. The reason for the change in the last run is not completely

understood. We speculate that some changes occurred in the film close to E_b. This reproducibility of the E_{oc} values is evidence that no irreversible electrochemical changes occurred in the film during the experimental procedure.

Table I
Polarization Experiments of Al

Specimen	1	2	3
Solution	KCl	KCl	Na_2SO_4
Overpotential (mV)	E_{oc}	E_{oc}	E_{oc} (mV,SCE)
0	-1511	-1500	-1551
200	-1507	-1468	-1539
400	-1521	- 1526	-1548
600	-1555	-1526	-1525
800	-1568	-1585	-1570
1000	-1526	-1545	
to E_b	-1371	-1508	
E_b (mV,SCE)	-581	-488	

Representative Al 2p spectra for the pure Al specimens immersed in the two electrolytes are shown in Fig. 4. They show that the as-received specimen is covered with only a very thin oxidized film as indicated by the relatively intense metallic Al peak at ~72 eV. The composition of this film is intermediate between Al_2O_3 and AlOOH. As the specimens are immersed and polarized in either electrolyte, the passive film thickens until the metallic peak can no longer be detected, corresponding to a thickness greater than ~10 nm, as determined by exponential-attenuation calculations using 2 nm as the attenuation length. At each overpotential, the film formed in the Na_2SO_4 solution is slightly thinner than that formed in the KCl solution. Compared to the as-received surfaces, the ones that have been immersed in an electrolyte are slightly more hydrated and are close to AlOOH in composition. These results are very similar to those we reported earlier for .99999 Al coupons (as opposed to these sputter-deposited thin films) in 0.05 M Na_2SO_4 at pH 7 with and without 1000 ppm Cl^- added.[14] A comparison shows that these

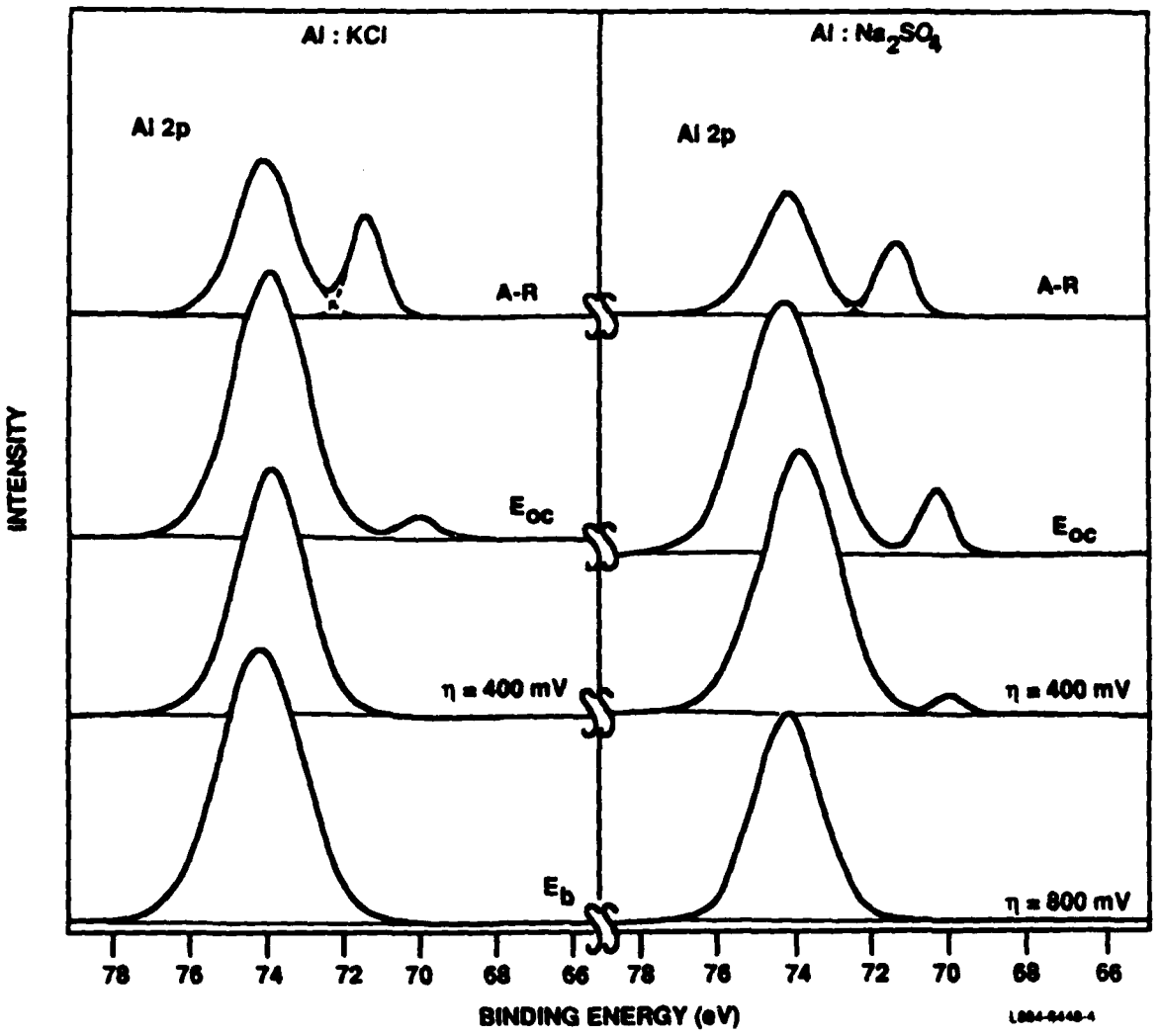

Figure 4. Al 2p XPS spectra from pure Al in either 0.1 M KCl or 0.1 M Na_2SO_4: as received (A-R), at E_{oc}, at overpotentials of 400 mV and 800 mV (Na_2SO_4-immersed specimen only), and at E_b (KCl-immersed specimen only).

sputter-deposited films behave identically to the bulk specimens and that the Na_2SO_4 electrolyte is benign. Except for possibly reducing film growth slightly, Na_2SO_4 does not affect the passive film to a significant degree at these overpotentials, in agreement with Augustynski.[1]

2. Al-Ta

Table II gives the values of E_{oc} for each polarization for the different Al-Ta specimens. These specimens exhibit E_{oc}'s that are 200-300 mV higher than those for pure Al (Table I). Again each specimen returns to approximately the same E_{oc} prior to retesting, which indicates that no irreversible changes occurred during measurement and storage. In the KCl solution, E_{oc} may depend on the alloy solute concentration as suggested by differences in the first two specimens; however, the range of solute concentrations used here is small, and thus no definitive conclusion can be reached. Earlier, such a dependence was found for Al-Mo, but not Al-Cr.[7] Additional comparison with Table I shows that E_b is 450-550 mV greater than that of pure Al, reflecting the alloy's superior passivity.

Selected Ta 4f and Al 2p spectra for Al-Ta alloys immersed and polarized in KCl and Na_2SO_4 are shown in Figs. 5 and 6, respectively. Quantitatively, the data are presented in Figs. 7 and 8 as a function of applied overpotential. Again, the as-received specimens have only a very thin passive film. This film is almost entirely oxidized aluminum; there is only a trace amount of oxidized Ta present. This characterization dramatically changes upon immersion and polarization in the electrolytes. The film becomes enriched in Ta_2O_5 beginning at E_{oc} and continuing until E_b, as shown by the ratio of oxidized Ta to oxidized Al given in Fig. 9, which also includes similar qualities for Al-Zr and Al-Cr.[7] The figures show that the enrichment is greater for the specimens immersed in Na_2SO_4 and after an overpotential of ~1000 mV, there is more Ta present in the passive film than Al. This trend of increased oxidized solute with overpotential is similar to that observed for Al-Cr, except that the increase appears more abrupt for Al-Cr. In contrast, no such trend was observed for Al-Mo.[7]

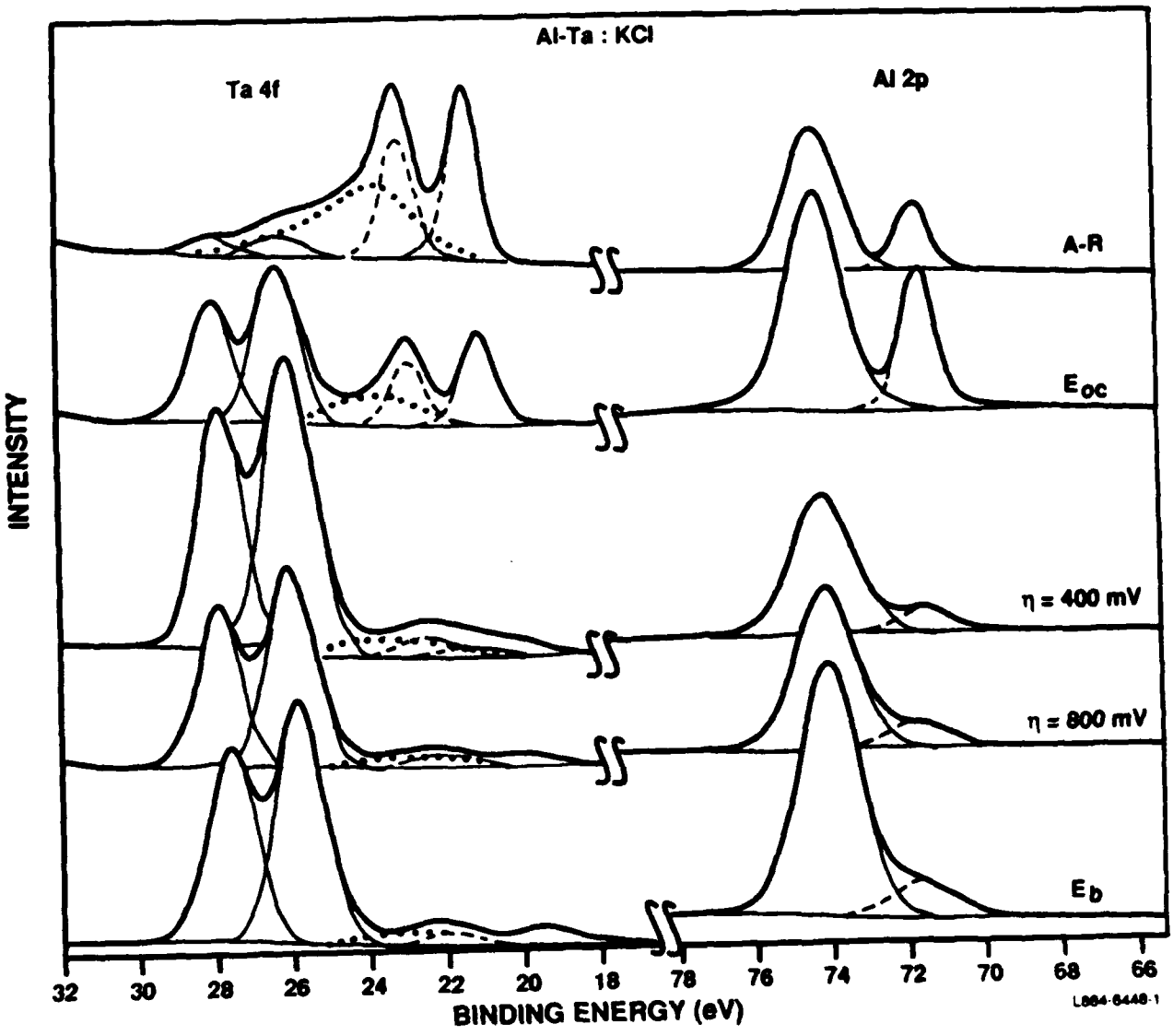

Figure 5. Ta 4f and Al 2p XPS spectra from an Al-Ta alloy in 0.1 M KCl: as received, at E_{oc}, at overpotentials of 400 mV and 800 mV, and at E_b. The dotted curve represents the O 2s peak. The thin, solid curves represent the oxidized states, whereas the dashed curves represent the metallic states. The two Ta peaks for each state correspond to the $4f_{7/2}$ and $4f_{5/2}$ spin-orbit-split components.

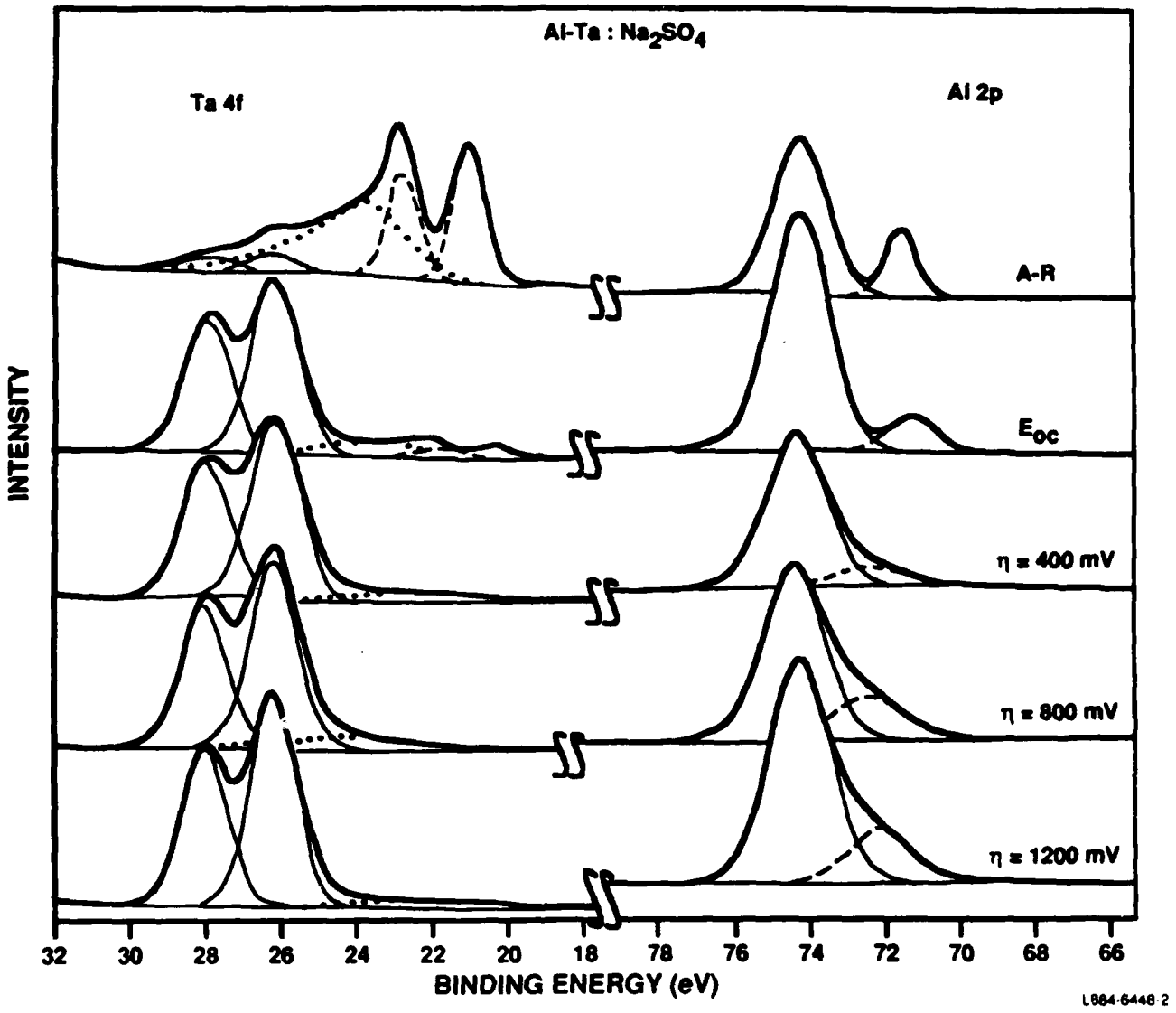

Figure 6. Ta 4f and Al 2p XPS spectra from an Al-Ta alloy in 0.1 M Na_2SO_4: as received, at E_{oc}, and at overpotentials of 400 mV, 800 mV, and 1200 mV. The dotted curve represents the O 2s peak. The thin, solid curves represent the oxidized states, whereas the dashed curves represent the metallic states. The two Ta peaks for each state correspond to the $4f_{7/2}$ and $4f_{5/2}$ spin-orbit-split components.

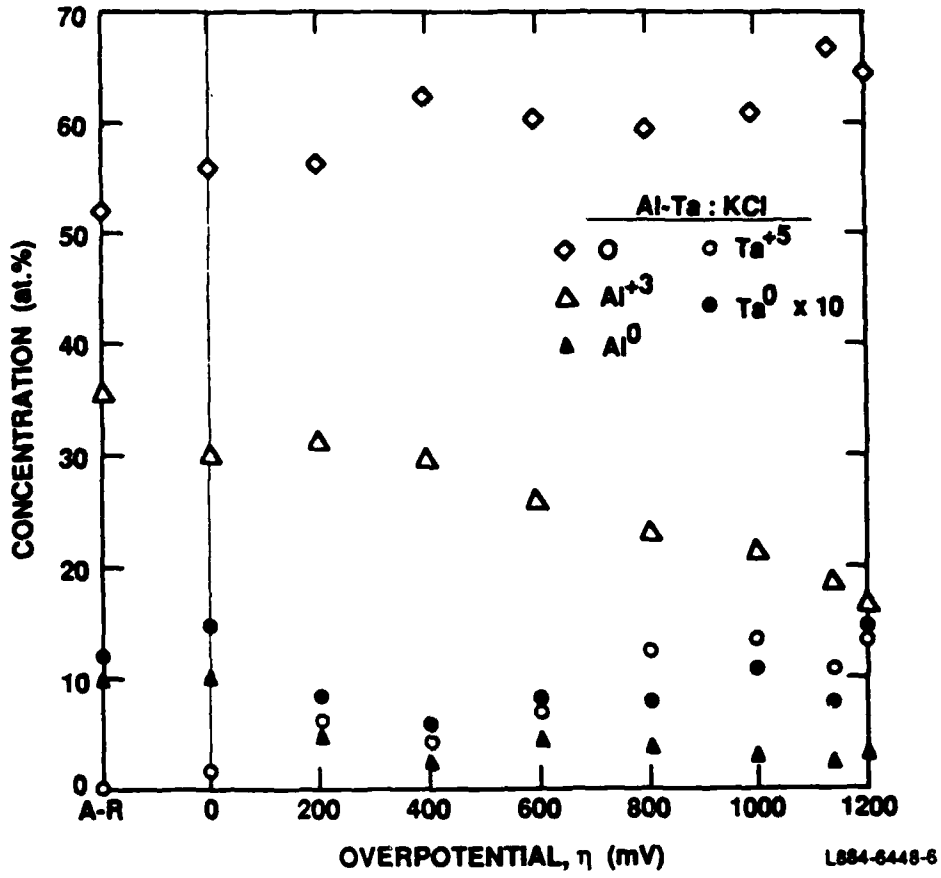

Figure 7. Surface composition, as determined by XPS, as a function of overpotential for the Al-Ta alloy in 0.1 M KCl.

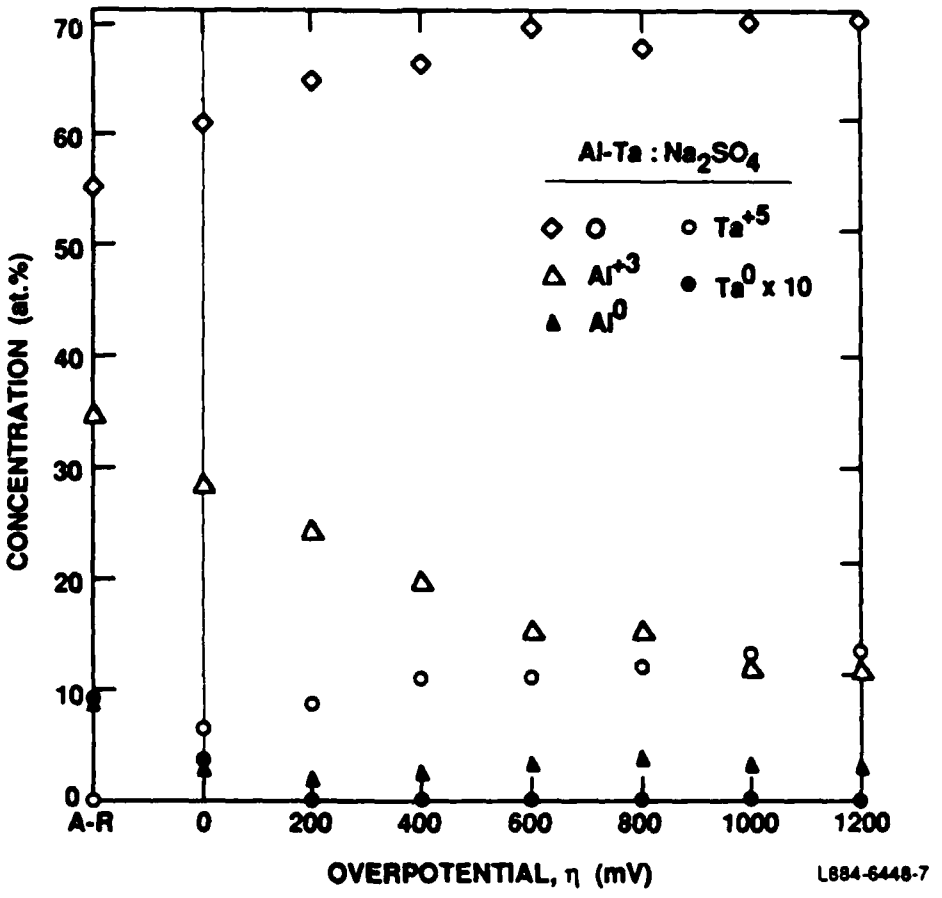

Figure 8. Surface composition, as determined by XPS, as a function of overpotential for the Al-Ta alloy in 0.1 M Na_2SO_4.

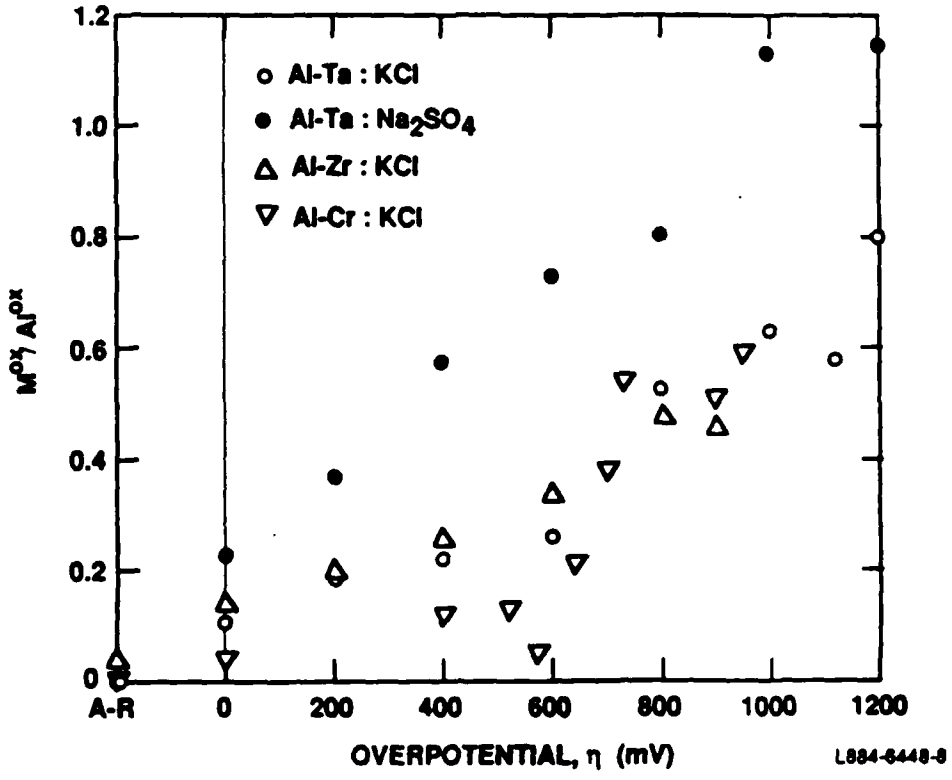

Figure 9. Ratio of the oxidized solute to oxidized Al, determined by XPS, as a function of overpotential for Al-Ta, Al-Zr, and Al-Cr alloys in 0.1 M KCl and for Al-Ta in 0.1 M Na_2SO_4.

Table II

Polarization Experiments with Al-Ta Alloys

Specimen	1	2	3	4
Ta conc. (at.%)	8	6	8	8
Solution	KCl	KCl	Na_2SO_4	Na_2SO_4
Overpotential (mV)	E_{oc}	E_{oc}	E_{oc}	E_{oc} (mV.SCE)
0	-1252	-1309	-1319	-1311
200	-1261	-1315	-1323	-1310
400	-1297	-1324	-1307	-1275
600	-1279	-1264[a]	-1255	-1281
800	-1227		-1242	-1223
1000	-1162		-1250	-1223
1200	-1228		-1229	-1198
to E_h	-1181			
E_h (mV, SCE)	-44			

[a] Experiment discontinued when specimen cracked.

An important difference between the passive films on the Al- Ta specimens and those on Al, Al-Cr, and also, as we shall see, on Al-Zr, is that the former are thinner, so that the metallic Al peak continues to be detected even at the highest overpotentials. In Na_2SO_4, the Al-Ta passive film thickens slightly upon immersion with no externally applied potential and changes little during anodic polarization. We estimate that it grows from ~4 nm before immersion to ~6 nm. In KCl, the passive film exhibits a similar behavior, except that it does not grow in thickness until an overpotential is applied.

Because the metallic region below the passive film can be examined by the XPS measurements, we can observe a difference in the Al-Ta specimens polarized in the two electrolytes. Throughout the polarization sequence, we can detect metallic Ta in the specimens exposed to the KCl solution. In fact, relative to metallic Al, the metallic Ta in the film-substrate interfacial region steadily increases in concentration with increasing potential (Fig. 10), suggesting that Al

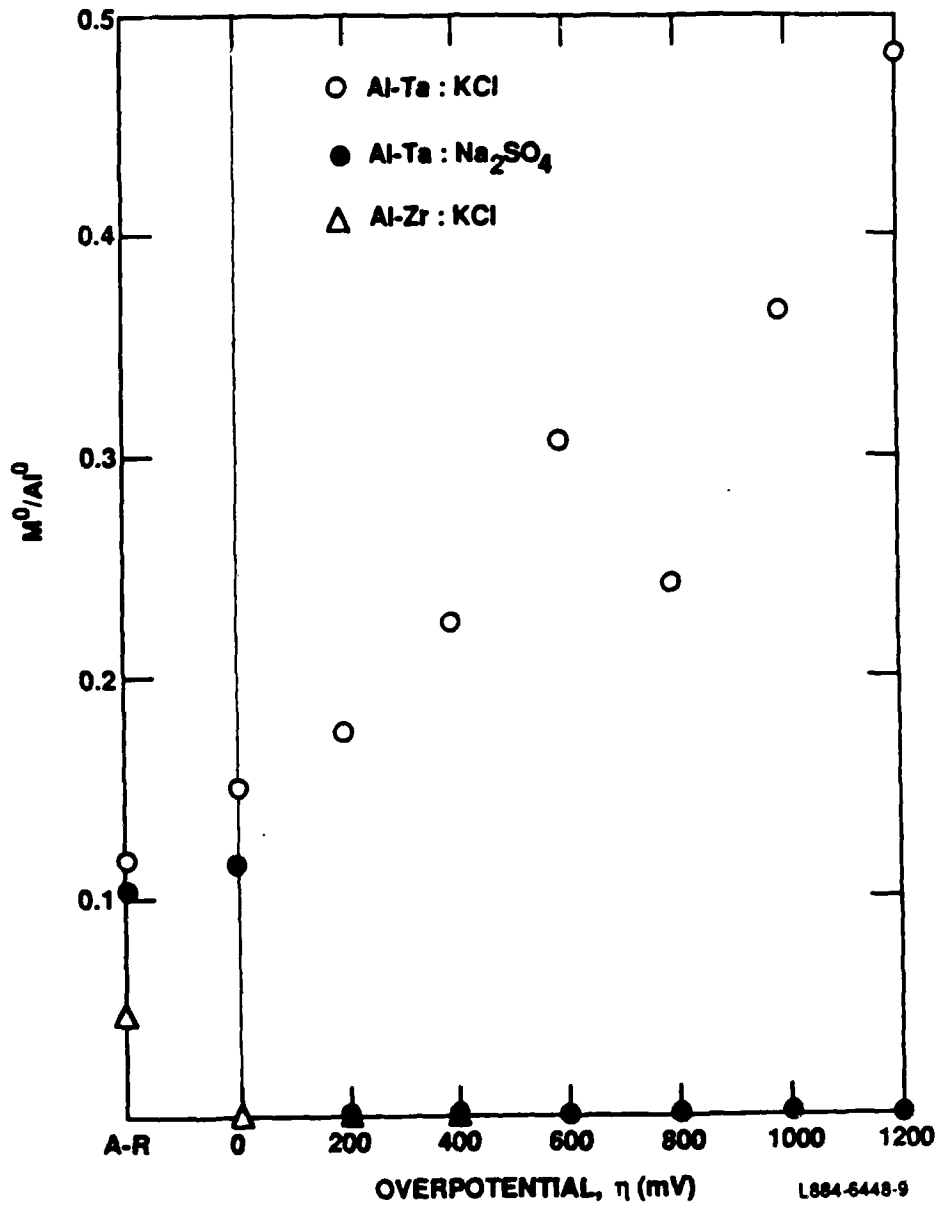

Figure 10. Ratio of the metallic solute to metallic Al, determined by XPS, as a function of overpotential for Al-Ta and Al-Zr alloys in 0.1 M KCl and for Al-Ta in 0.1 M Na_2SO_4.

is being preferentially oxidized similar to Al-Cr and Al-Mo. This is not the case for specimens immersed in Na_2SO_4. Although the metallic Al peak is detected at each overpotential, the metallic Ta peak is lost under the O 2s peak after the first polarization (Figs. 5 and 10). Clearly, Ta is not enhanced at the interface in Na_2SO_4 as it is in KCl; however, because of the interference with the O peak (and the subsequent loss of sensitivity for metallic Ta), we cannot distinguish between a depletion of Ta just below the passive film and an interfacial concentration equal to the bulk value.

3. Al-Zr

Table III summarizes the polarization/surface analysis experiments for Al-Zr. Again we see reproducibility in E_{oc} with the values approximately 100 mV more noble than those of pure Al. The breakdown potential also increases by a similar amount compared with the pure material, resulting in relatively little improvement in passivity.

Table III
Polarization Experiments of Al-Zr Alloys

Zr Conc.(at.%)	4
Solution	KCl
Overpotential (mV)	E_{oc}(mV,SCE)
0	-1404
200	-1366
400	-1396
600	-1432
800	-1427
to E_b	-1363
E_b(mV,SCE)	-463

The Zr 3d and Al 2p spectra for the Al-Zr specimen are given in Fig. 11, and the surface composition is given as a function of applied potential in Fig. 12. As with the other alloys investigated to date, Al is preferentially oxidized in the atmosphere and the air-formed passive

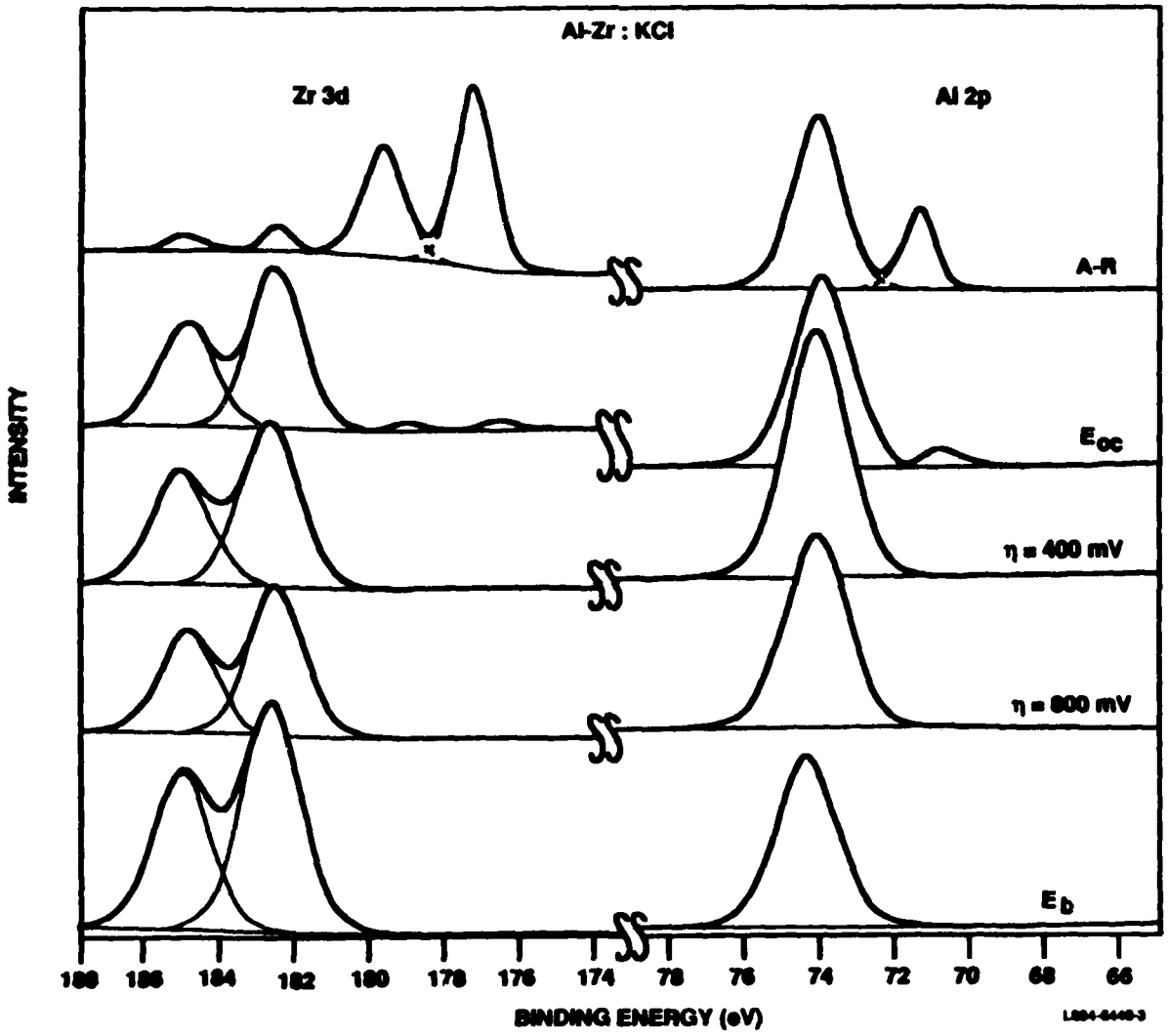

Figure 11. Zr 3d and Al 2p XPS spectra from an Al-Zr alloy in 0.1 M KCl: as received, at E_{oc}, at overpotentials of 400 mV and 800 mV, and at E_b. The solid curves represent the oxidized states whereas the dashed curves represent the metallic states. The two Zr peaks for each state correspond to the $3d_{5/2}$ and $3d_{3/2}$ spin- orbit-split components.

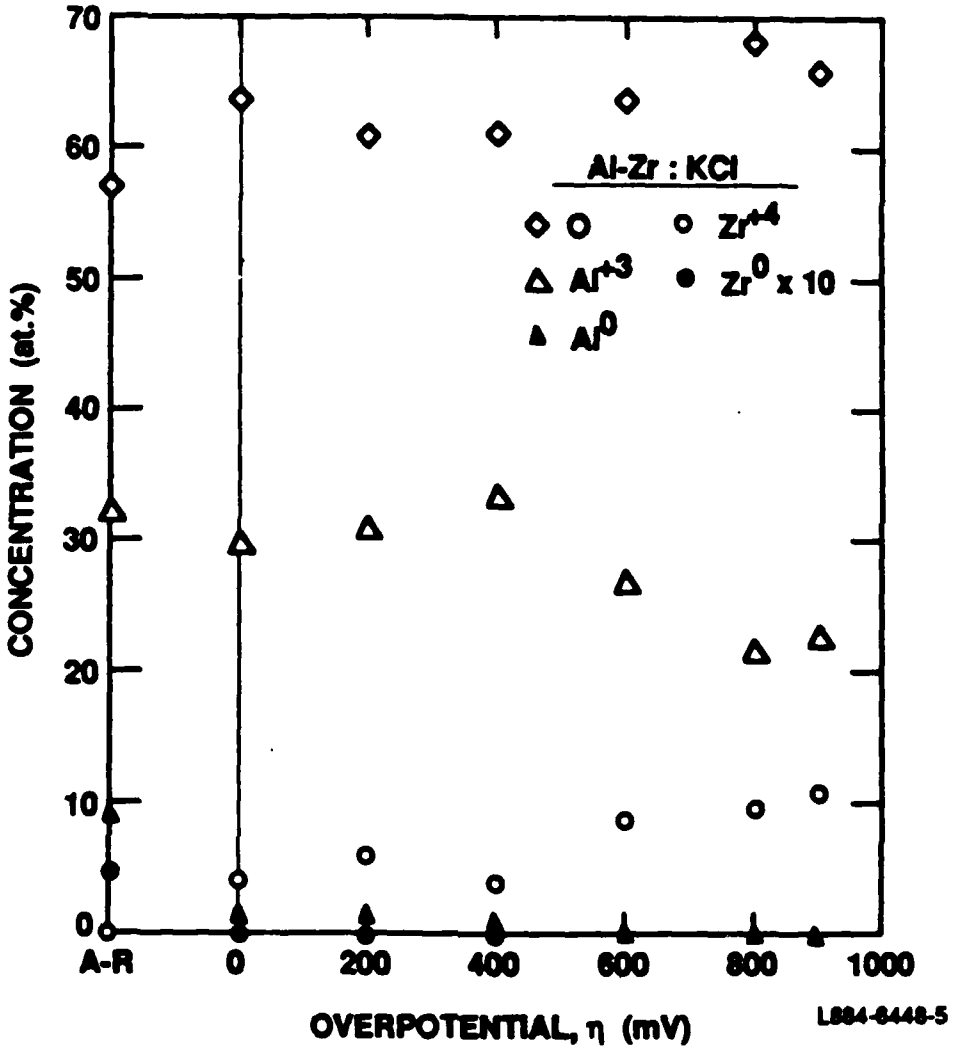

Figure 12. Surface composition, determined by XPS, as a function of overpotential for the Al-Zr alloy in 0.1 M KCl.

film contains little solute. Upon immersion in the electrolyte, the passive film thickens and the solute is also oxidized. Like the Al, Al-Mo, and Al-Cr specimens, the passive film quickly thickens upon polarization, and the metallic peaks are no longer detectable. The film becomes increasingly enriched in oxidized Zr until it is nearly one-half ZrO_2 (Fig. 9).

D. PASSIVE FILM STRUCTURE

The reflectivity spectra of an Al-6Mo alloy specimen polarized to -400 mV (SCE) is shown in Fig. 13 and can be compared to those of α-Al_2O_3 (sapphire) given in Fig. 14. Each of the Al-Mo specimens measured (Al-6Mo, Al-9Mo, and Al-13Mo) gave nearly identical results. This is consistent with the XPS analysis, which showed that each passive film consisted primarily of oxidized Al, with little oxidized Mo. Qualitatively, the passive films look very similar to α-Al_2O_3; the most notable difference being a decrease in the resolution of the Fourier transform caused by the less ordered nature of the passive film, and the resulting broadening of the radial-distribution function for the same Fourier resolution.

Table IV lists the nearest neighbor distances for the three alloys and a sapphire standard.

Table IV
Oxygen to Metal Atom Distances of Al-Mo Alloys

Specimen	O-M Distance (nm)
Sapphire	0.169
Al-6Mo	0.168 ± .002
Al-9Mo	0.168 ± .002
Al-13Mo	0.167 ± .002

(a)

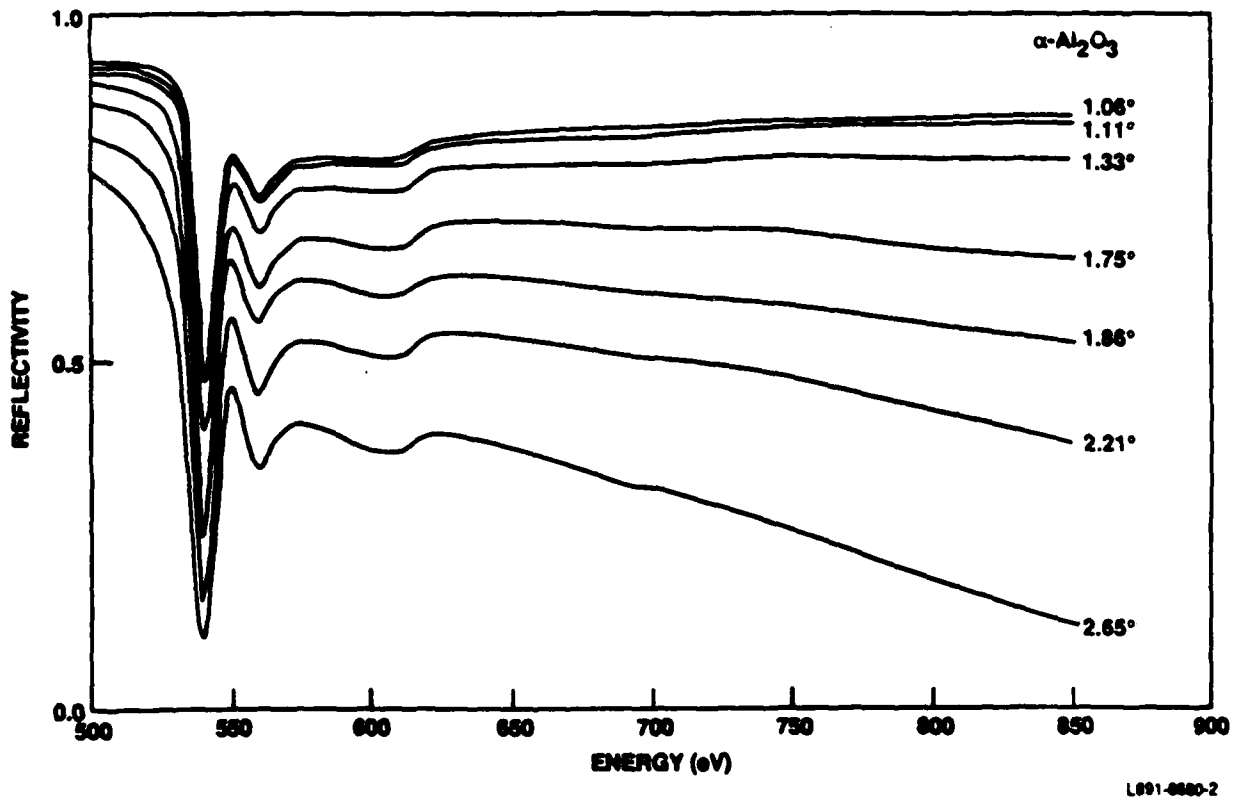

Figure 13. Reflectivity (a), EXAFS function (b), and radial distribution function (c) for the Al-6Mo passive film formed at -400 mV (SCE).

(b)

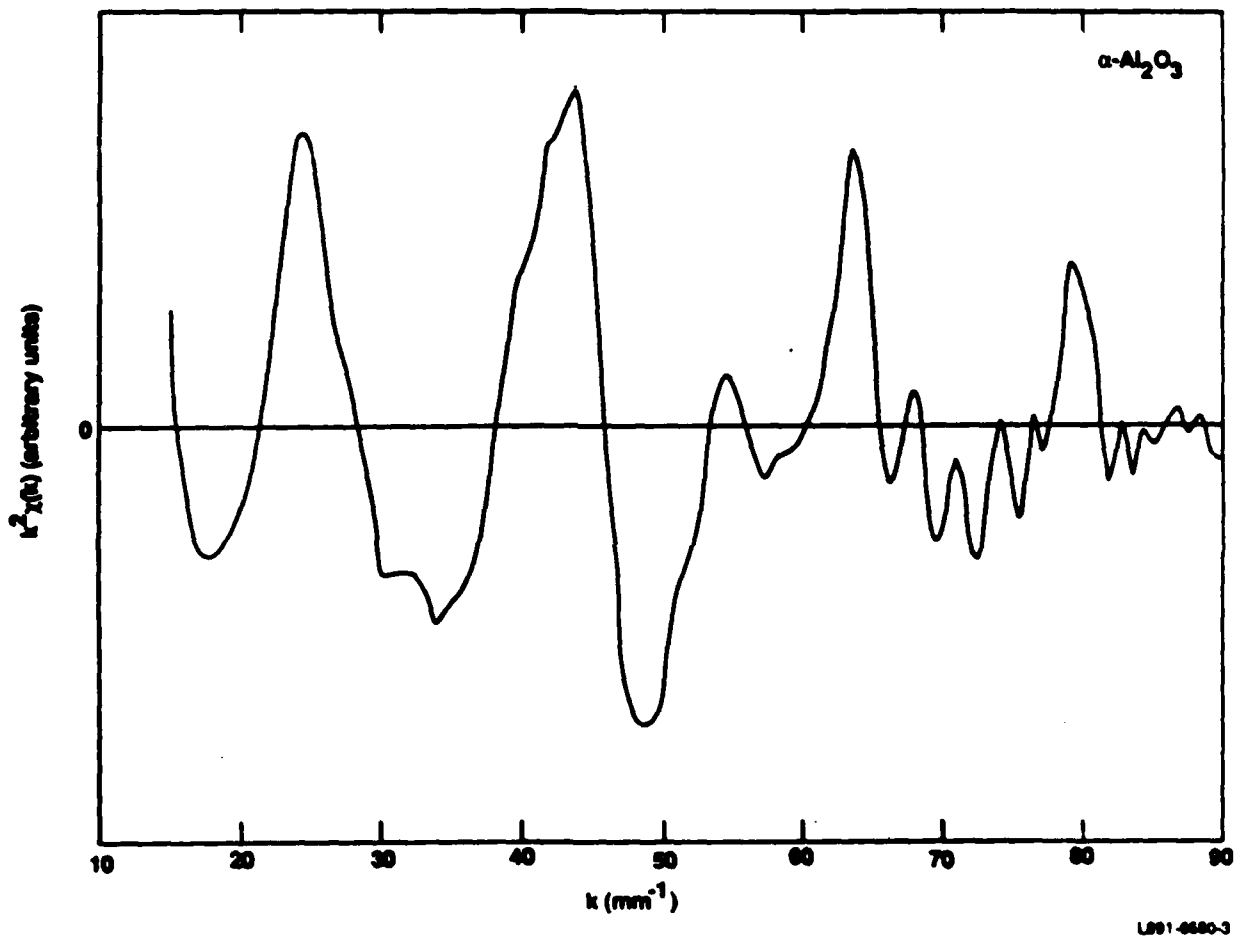

Figure 13 (continued)

(c)

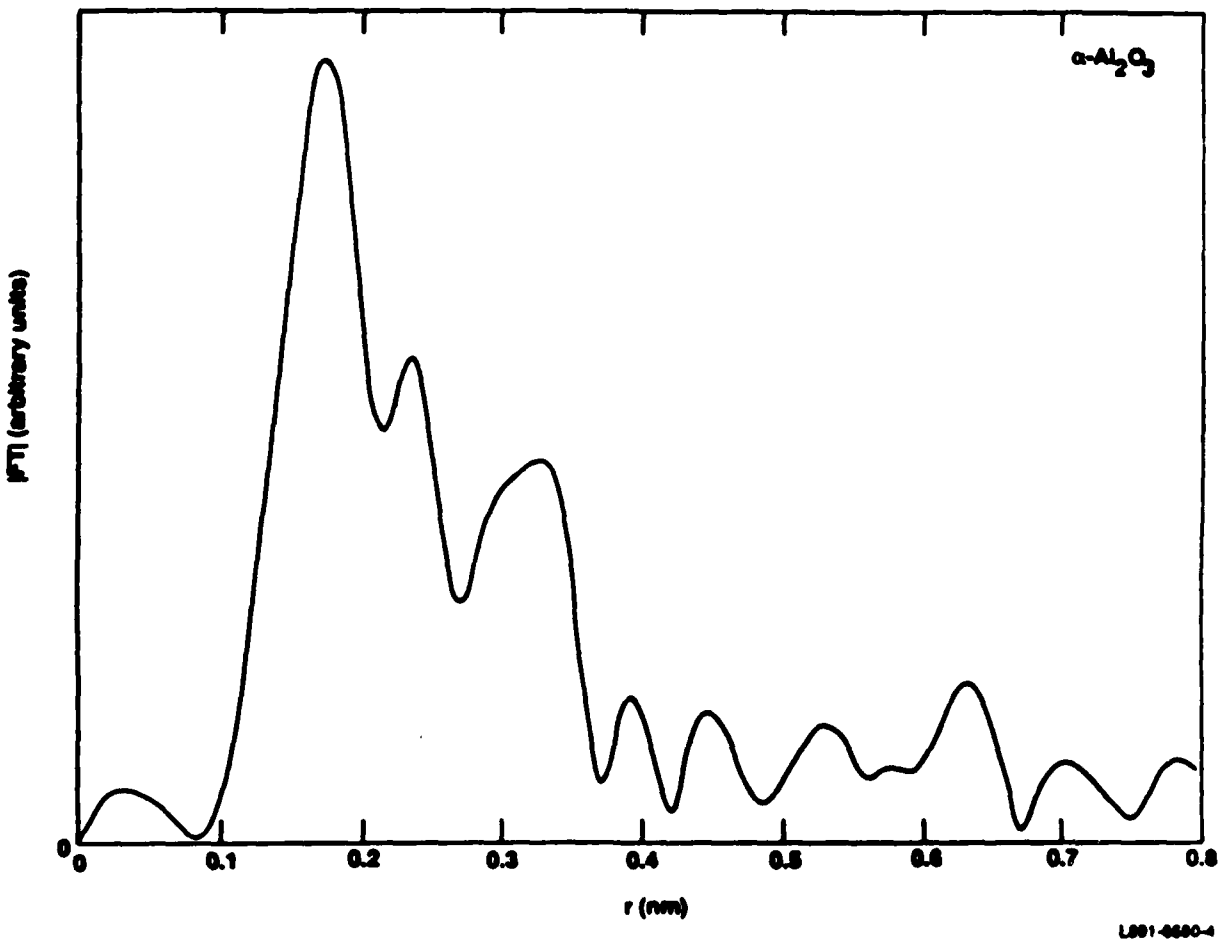

Figure 13 (continued)

(a)

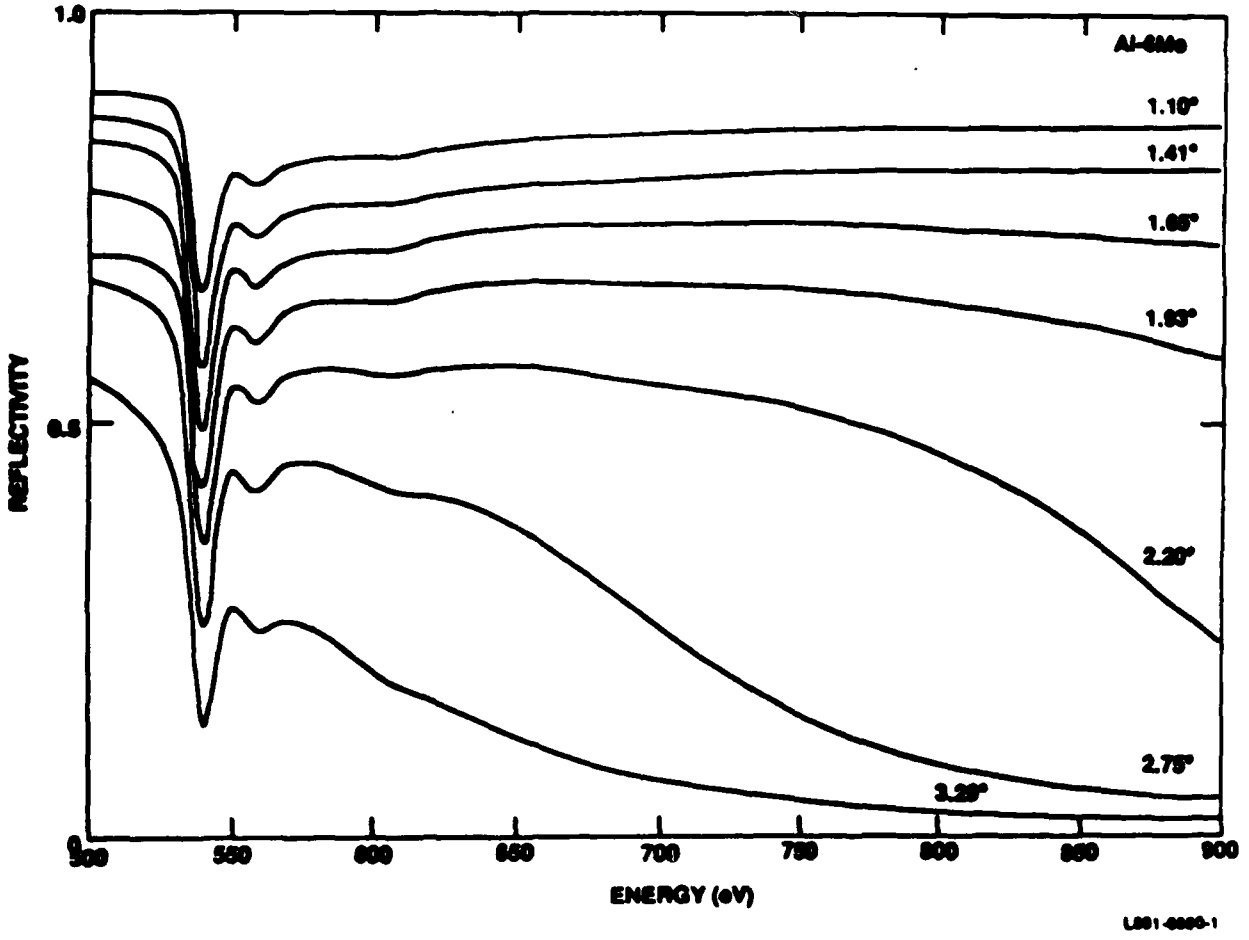

Figure 14. Reflectivity (a), EXAFS function(b), and radial distribution function (c) for α-Al_2O_3.

(b)

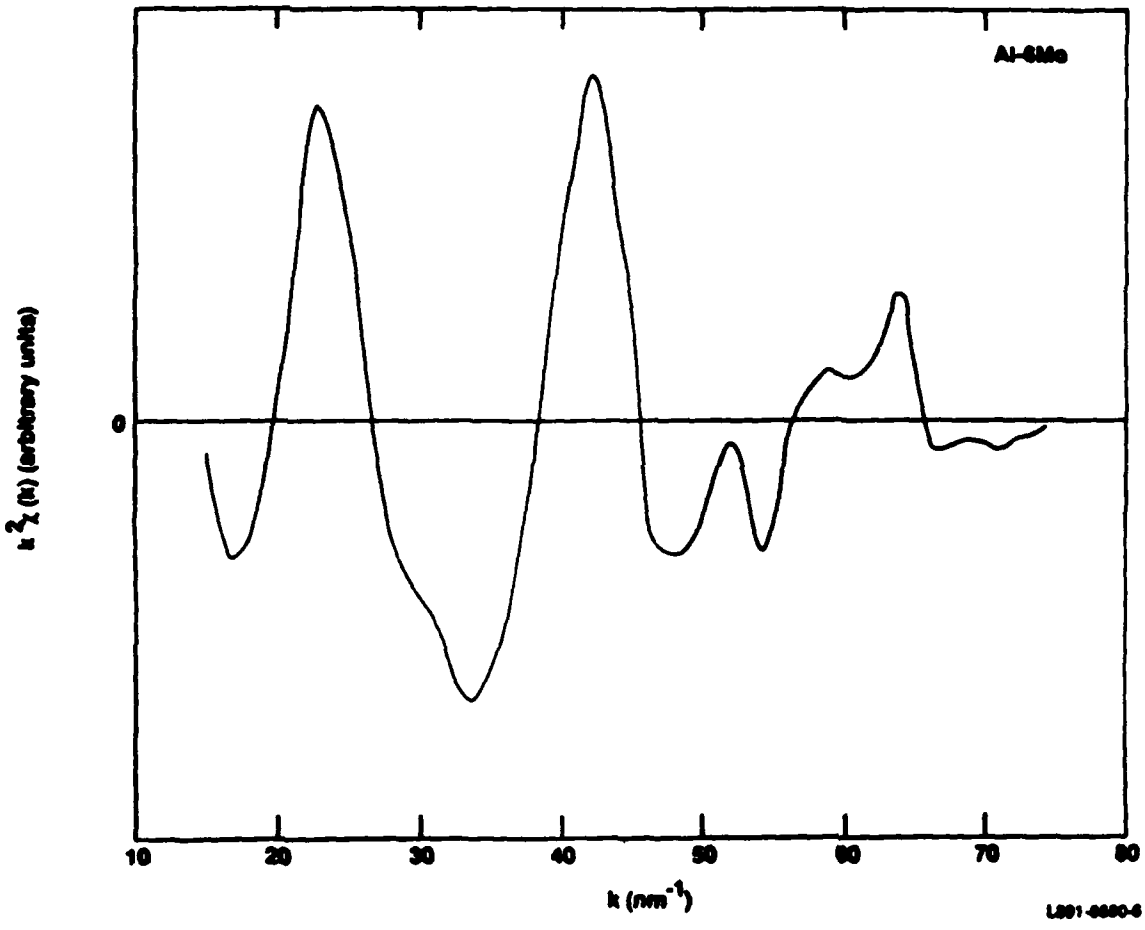

Figure 14 (continued)

(c)

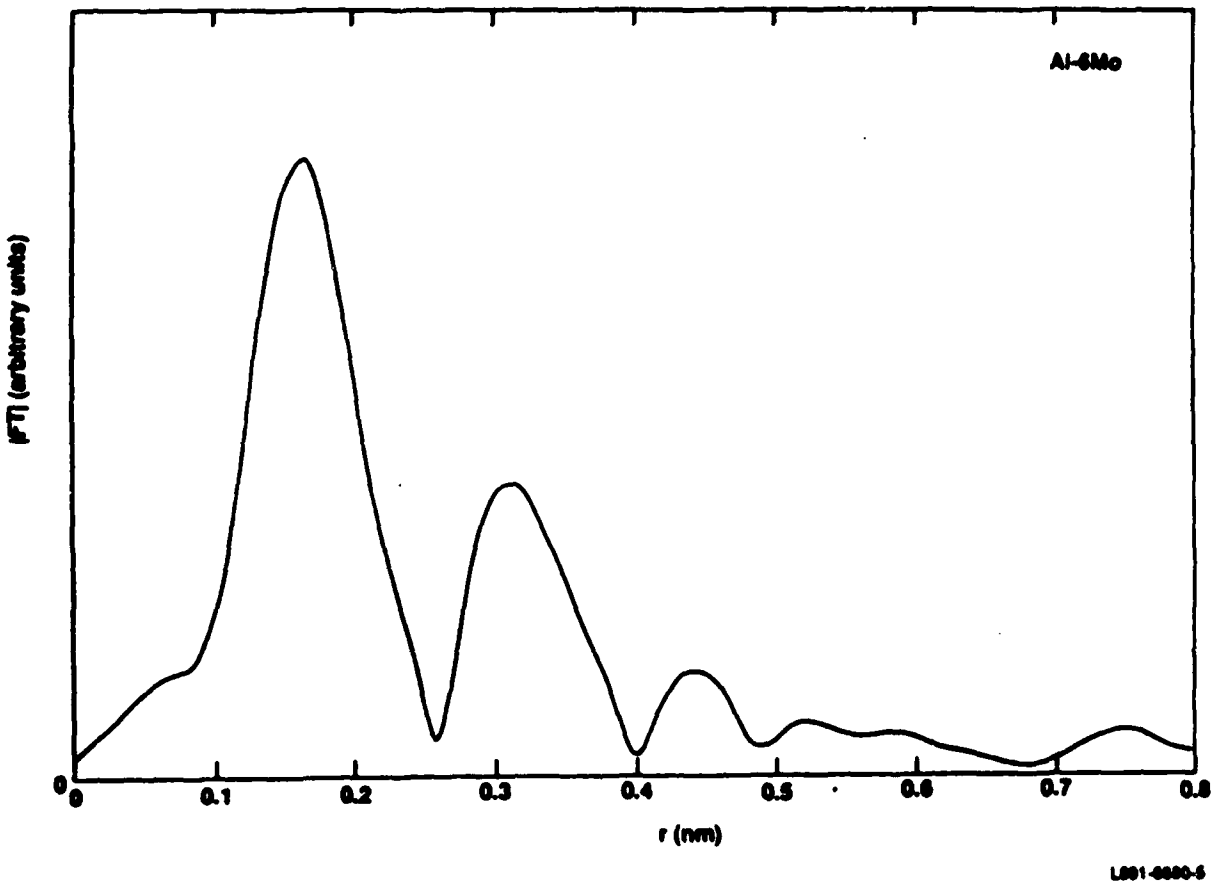

Figure 14 (continued)

IV. DISCUSSION

Of the six alloys reported here, Al-Ta, Al-Zr, Al-Mo, and Al-Cr alloys each exhibited superior corrosion behavior compared with pure Al. The poor performance of Al-Cu was probably caused by $CuAl_2$ precipitates, which promote localized attack. This was the only alloy which XRD indicated that precipitation had occurred at room temperature. The low E_b value we obtained for the Al-Si alloy is surprising, considering that Natishan et al.[12] found that Al-Si had one of the highest E_b values among all the ion-implanted alloys they investigated. The discrepancy can be attributed to the low concentration of Si (≤1 at.%) in our co-sputter-deposited alloys. The sputtering rate of Si is so low compared will that of Al that we were only able to obtain a very dilute solid solution.

The corrosion inhibition of these alloying elements is achieved only as long as they are maintained in solid solution so that the alloy is metallurgically homogeneous. Once precipitates are formed, e.g., during heat treatment, breakdown can occur at or near these heterogeneities. Earlier experiments with Al-Mo alloys that had been heated showed that numerous small pits spontaneously formed in KCl solutions.[21] Of all of the alloys studied, only Al-Ta continued to exhibit resistance to salt fog attack following heat treatment and the resulting nucleation of an intermetallic phase (Al_3Ta). One possible explanation is that there might be a very small potential difference between the Al_3Ta intermetallics and the matrix that does not promote the formation of local galvanic cells. However, the potential difference between the two phases is not known.

The comparison between the humidity tests and the salt fog and potentiodynamic tests shows that the several of the solutes are very effective in inhibiting attack by Cl^-, but do not significantly inhibit hydration. The passive films and then the underlying metal itself transformed first to AlOOH and then to $Al(OH)_3$.[17,22] However, this hydration could be stopped (or, at least, slowed substantially) with an organosilane treatment.[23] The organosilanes form a fused polymeric network on the surface[24] similar to that which protects conventional aluminum alloys from hydration.[19,20] The organosilane treatment has also been shown to inhibit localized attack in conventional alloys immersed in KCl,[20] but to a much lesser extent than these solutes inhibit attack.

The behavior of the Al-Ta and Al-Zr alloys in the deaereated KCl solution is similar in many senses: Only one oxidized form of the solute, i.e., Ta_2O_5 or ZrO_2, respectively, is present within the film. Conversely, up to three different oxidized states were present in Al-Mo and Al-Cr. The amount of oxidized solute is very small initially and increases with applied potential -- slowly at first and then more rapidly at overpotentials greater than ~600 mV (Fig. 9). On the other hand, one important difference is that the passive film on Al-Ta remains thin throughout the polarization sequence, whereas the film on Al-Zr (and Al, Al-Mo, and, at a slower rate, Al-Cr) thickens until it is the only constituent in the XPS detection volume.

As we discussed in connection with the Al-Mo alloys,[5-7] the high-exchange current density for the hydrogen reaction on Ta[25] indicates that Ta also would not impede the growth of a pit, but must instead control pit nucleation. The situation for Zr is less clear, but the same argument is likely to be true here also. To control pit nucleation, these alloying additions must either reduce the adsorption of Cl^- onto the surface, inhibit the reaction between the adsorbed Cl^- with the passive film, or impede the transport of Cl^- through the film or, alternatively, the dissolution of the film.[26]

The first possible mechanism (reduction of Cl^- adsorption) is consistent with the lack of Cl (<0.5 at.%) found on our surfaces. However, unlike Augustynski,[1] who reported 3 at.% Cl at E_{oc} and 12 at.% Cl at E_b (as measured by XPS), we find no more than trace quantities on our pure Al surfaces at any potential. Because the differences in adsorption between our alloy surfaces and our control surface are too small to measure, we suggest that the adsorption of Cl^- is not the controlling step in the passivity of our alloys.

The improvements in the pitting behavior, then, is likely to be controlled by another mechanism, at least in part. Earlier, we showed that the reaction between adsorbed Cl^- and Al-Mo and Al-Cr surfaces was identical to that occurring on pure Al surfaces, and that the corrosion resistance is provided by a molybdate or CrOOH region of the passive film that acts as a barrier to Cl penetration to the substrate.[7,27] The same mechanism is likely to control the passivity of Al-Ta and Al-Zr films as well. In the case of Al-Cr passive films, the CrOOH barrier also impeded the ingress of oxygen and the films were thinner than those of the control. The Ta_2O_5 in the Al-Ta passive film is considerably more efficient at blocking oxygen from the metal substrate and thus preventing the substrates' subsequent oxidation. Consequently, the substrate remains visible to XPS throughout the polarization sequence. The increase in the

relative amount of metallic Ta present at the interface indicates that Al is being preferentially oxidized as the applied potential is increased. The simultaneous increase in the relative amount of oxidized Ta present in the passive film suggests that the Al in the film is going into solution, possibly in the form of $AlCl_3$. In the Na_2SO_4 solution, the combined effect of the absence of significant dissolution of Al into the electrolyte and the presence of more oxidized Ta, which impedes oxygen ingress to the substrate, results in less oxidation and consequently no build-up of metallic Ta at the interface.

What then causes the eventual breakdown of the Al-Ta passive film? In Al-Cr, we attributed this to the further oxidation of the CrOOH to the more soluble CrO_3, which allowed Cl access to the substrate. We see no evidence for a similar change in the Ta chemistry to allow localized attack. Rather, we attribute breakdown to the thinness of the passive film. As the potential is increased, the electric field across the film acts as a driving force for negatively charged ions. Eventually, the Ta_2O_5 is unable to prevent the transport of Cl^- through the film to the substrate and pitting occurs.

In both Al-Zr and Al-Ta alloys, the solute possesses one common oxide and no change in the Zr or Ta chemistry is observed. However, the ZrO_2 in the passive film of Al-Zr specimens is less effective in blocking transport of chloride and oxygen to the substrate. As a result, the passive film is thicker throughout the polarization sequence and breakdown occurs at a lower potential, and thus only small improvements in the passivity are made relative to pure Al.

V. SUMMARY AND CONCLUSIONS

The corrosion behavior of Al and supersaturated Al-Mo, Al-Cr, Al-Zr, Al-Ta, Al-Si, and Al-Cu alloys have been examined using potentiodynamic polarization in deaerated and aerated KCl and salt-fog tests. The Al-Ta, Al-Mo, Al-Cr, and Al-Zr alloys each exhibited improved passivity compared to the control, pure aluminum, with the Al-Ta alloy possessing the highest breakdown potential. However, this increased passivity occurs only if the solute is maintained in solid solution. If the specimens are heated to induce precipitation, only the Al-Ta alloys passed the salt-fog test by remaining shiny after 3 days of exposure. Examination of the evolution of the passive film chemistry during anodic polarization showed that the passive film of Al-Ta alloys becomes increasingly enriched in oxidized solute (Ta_2O_5) as does Al-Zr, and Al-Cr alloys. In each of these cases and in that of Al-Mo alloys, an oxidized solute species restricts the transport of Cl^- through the oxide and inhibits breakdown. Tantalum is the most effective solute in this regard: not only does it exhibit the greatest E_b, but it also restricts the ingress of oxygen to the substrate to prevent the passive film from growing in thickness. Breakdown occurs only when the potential drop across the film becomes great enough to allow the transport of chloride.

ACKNOWLEDGEMENTS

We gratefully acknowledge the help of J.G. Slunt and S.W. Duncan in the preparation of these sputter-deposited alloy films and valuable discussions with J.S. Ahearn and B.A. Shaw. This program was funded by A.J. Sedricks of the Office of Naval Research under contract no. N00014-85-C-0638.

REFERENCES

1. J. Augustynski, in Passivity of Metals, edited by R.P. Frankenthal and J.Kruger, p. 973, The Electrochemical Society, Princeton, NJ (1978).

2. R.R. Wiggle, V. Hospadaruk, and E.A. Styloglou, Mater. Perf. 20(6), 13 (1981).

3. M.S. Vukasovich and J.P.G. Farr, Mater. Perform., 25(5), 9 (1986).

4. W.C. Moshier and G.D. Davis, submitted to Corrosion.

5. W.C. Moshier, G.D. Davis, J.S. Ahearn, and H.F. Hough, J. Electrochem. Soc. 133(5), 1063 (1986).

6. W.C. Moshier, G.D. Davis, J.S. Ahearn, and H.F. Hough, J. Electrochem. Soc. 134(11), 2677 (1987).

7. W.C. Moshier, G.D. Davis, and G.O. Cote, J. Electrochem. Soc. 136(2), 356 (1989).

8. W.C. Moshier, G.D. Davis, T.L. Fritz, and S.W. Duncan (to be published).

9. A.H. Al-Saffar, V. Ashworth, A.K.O. Bairamov, D.J. Chivers, W.A. Grant, and R.P.M. Procter, Corr. Sci. 20(1), 127 (1980).

10. P.M. Natishan, E. McCafferty, and G.K. Hubler, J. Electrochem. Soc. 133(5), 1061 (1986).

11. E. McCafferty, G.K. Hubler, P.M. Natishan, P.G. Moore, R.A. Ka, and B.D. Sartwell, Mater. Sci. Eng. 86(1), 1 (1987).

12. P.M. Natishan, E. McCafferty, and G.K. Hubler, J. Electrochem Soc. 135(2), 321 (1988).

13. W.C. Moshier, G.D. Davis, and J.S. Ahearn, Corros. Sci. 27, 785 (1987).

14. G.D. Davis, W.C. Moshier, J.S. Ahearn, H.F. Hough, and G.O. Cote, J. Vac. Sci. Technol. A 5(4), 1152 (1987).

15. G.G. Long and J. Kruger, in Techniques for Characterization of Electrodes and Electrochemical Proceses, edited by R. Varma and J.R. Selman (Wiley, New York, in press).

16. J.S. Ahearn, G.D. Davis, T.S. Sun, and J.D. Venables, in Adhesion Aspects of Polymeric Coatings, edited by K.L. Mittal (Plenum, New York, 1983), p. 281.

17. G.D. Davis, J.S. Ahearn, L.J.Matienzo, and J.D. Venables, J. Mater. Sci. 20, 975 (1985).

18. F.J. Boerio and R.G. Dillingham, in Adhesive Joints: Formation Characteristics and Testing, edited by K.L. Mittal (Plenum, New York, 1984), p. 541.

19. F.J. Boerio, R.G. Dillingham, and R.C. Bozian, in Proceedings of 39th Annual Conference of Reinforced Plastics/Composites Institute, Houston, January 1984, Session 4-A, p. 1.

20. L.J. Matienzo, D.K. Shaffer, W.C. Moshier, and G.D. Davis, J. Mater. Sci. 21, 1601 (1986).

21. W.C. Moshier, G.D. Davis, J.S. Ahearn, and H.F. Hough, "Corrosion Behavior of Sputter-Deposited Aluminum-Based Alloys Containing Molybdenum or Chromium Exposed to Chloride Solutions," Martin Marietta technical report no. TR 86-79c (unpublished).

22. G.D. Davis, T.S. Sun, J.S. Ahearn, and J.D. Venables, J. Mater. Sci. 17, 1807 (1982).

23. E.P. Plueddemann, Silane Coupling Agents (Plenum Press, New York, 1982).

24. K.W. Allen, A.K. Hansrani, and W.C. Wake, J. Adhes. 12, 199 (1981).

25. J. West, Electrodeposition and Corrosion Processes, p. 56, Van Nostrand-Reinhold, London (1971).

26. R.T. Foley, Corrosion 42, 277 (1986).

27. W.C. Moshier, G.D. Davis, G.O. Cote, H.F. Hough, and M.E. Vogelsang, "Corrosion Behavior of Sputter-Deposited Aluminum-Base Alloys Exposed to Chloride Solutions," Martin Marietta technical report no. TR 87-75c (unpublished).

APPENDIX

REFLEXAFS

Among the various structural probes of passive films, extended x-ray absorption fine structure (EXAFS) spectroscopy is a particularly useful technique in that it is sensitive to short-range order about specific elemental species in disorder as well as crystalline materials. Using EXAFS, radial distribution functions can be derived about one or more atomic speicies without solving the entire structure.

EXAFS generally occurs 50 to 1000 eV above an x-ray absorption edge -- a spectral region where the fine structure results from the interference of the outgoing electron waves with the waves backscattered by the neighboring atoms in the photoionization process.[A1] Consequently, it can be simply related to the atomic arrangement around the absorbing atom. The absorption cross section for the photoexcitation of a K-shell electron in a material $\mu(E)$ can be expressed as

$$\mu(E) = \mu_b + \mu_0(E)|\,1+\chi(k)|, \qquad (1)$$

where μ_0 is the free-atom absorption coefficient for the core level of interest, μ_b is the background absorption coefficient due to electrons from all other levels, and $k=2\pi[2m(E-E_0)]^{1/2}/h$ is the photoelectron momentum. The EXAFS function, $\chi(k)$, depends on the number of neighboring atoms, N_i, at distance, r_i, from the absorbing atoms, on the backscattering amplitude, $f_i(k)$, and on the phase shift due to the atomic potentials, $\psi_i(k)$:

$$\chi(k) = \Sigma_j\, A_j(k)\sin(2kr_j+\psi_j(k)) \qquad (2)$$

with

$$A_j(k) = N_j/(kr_j^2)f_j(k)S_0^2\exp(-2k^2\sigma^2-2r_j/\lambda) \qquad (3)$$

where S_0^2 is the amplitude reduction factor that accounts for the relaxation of the absorbing atom and multiple electron excitations, σ^2 is a Debye-Waller-like parameter that accounts for the mean-square relative positional fluctuations of the atoms due to either structural disorder or

thermal vibrations, and λ is the electron mean free path. The sum is over the j neighboring atomic shells in the material. The phase shifts are generally derived by comparing the experimental phase shifts with those measured from model compounds, or by fitting the filtered and backscattered peak in the Fourier transformed $\chi(k)$.

The Fourier transform of the EXAFS function leads to the determination of structural parameters:

$$P(r) = (1/2\pi)^{1/2} \int_{k_{min}}^{k_{max}} k_n \chi(k) \exp(2ikr) dk \,. \qquad (4)$$

The factor k_n is used to emphasize the weight of the higher k region of the EXAFS spectrum. Usually, n is between 1 and 3 depending on the weighting needed to equalize the amplitude dependence.

The bond distances that are derived from EXAFS data are generally accurate to about 1-2% with the greatest source of error being uncertainties in ψ, especially in the case of low-Z (C, N, O, etc.) absorbers and scatterers. By comparison, the derived coordination numbers, N, are only good to ~20% because other parameters, such as the disorder factors and the electron mean free path, also contribute to the amplitude.

In the practical application of EXAFS a physical quantity that is roughly proportional to $\mu(k)$ is commonly used instead of $\mu(k)$. In reflEXAFS, the measured quantity is the reflectivity of glancing incident x-rays.[A1,A2] Although the reflectivity is less simply related to $\mu(k)$ than are other processes, such as fluorescence, it provides excellent signal-to-noise and has very good surface sensitivity.

The reflectivity at small angles can be written

$$R = |(\phi-a)^2 + b^2|/|(\phi+a)^2 + b^2| \qquad (5)$$

with

$$a^2 = (1/2)\{[(\phi^2-\phi_c^2)^2 + 4\beta^2]^{1/2} + (\phi^2-\phi_c^2)^2\} \quad (6)$$

and

$$b^2 = (1/2)\{[(\phi^2-\phi_c^2)^2 + 4\beta^2]^{1/2} - (\phi^2-\phi_c^2)\} \quad (7)$$

where the critical angle, ϕ_c, is defined as

$$\phi_c = (2\delta)^{1/2} \quad (8)$$

and δ and β are contributions to the complex index of refraction

$$n = 1-\delta - \beta i. \quad (9)$$

These quantities are further related to the absorption coefficient by

$$\mu = 4\pi\beta(1-\delta)/\lambda. \quad (10)$$

Below the critical angle, total reflection occurs and only evanescent waves are present in the material with an e^{-1} penetration depth, d, of

$$d = \lambda/(4\pi b) \quad (11)$$

where λ is the wavelength of the radiation. The penetration depth for Al_2O_3 is given in Fig. A1 as a function of glancing angle for a range of energies near the oxygen K-edge. For angles less than ~2.3° (40 mrad), the penetration depth for photon energies up to 800 eV is less than 3 nm; at smaller angles, it is less.

The first step in data reduction is to remove the instrumental factors from the raw data over the range from 250 to 800 eV. A measure of the instrument function is provided by blank

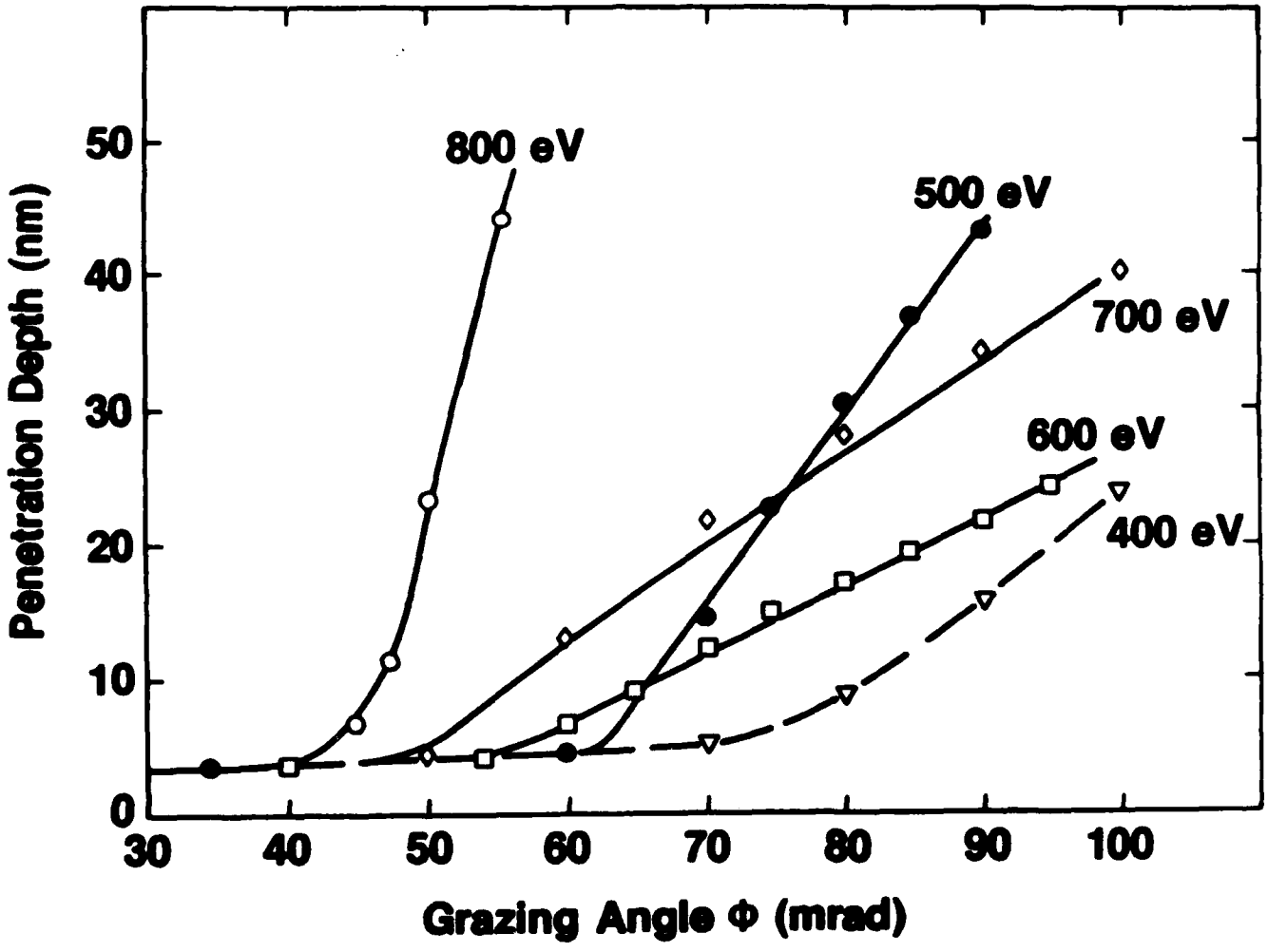

A1. Penetration depth as a function of incident angle for Al_2O_3 for photon energies around the O K edge.

scans, which are obtained without the sample present. This permits a quantitative measure of contamination in the optics, of the oxygen in the contamination barrier, and of the relative behavior of the phosphors and the detectors. Corrections to the measured intensities must be made because of the presence of second- and third-order harmonics. The relative second- and third-order content in the 250 to 700 eV region of the incident spectrum was provided using data obtained by means of a variable absorber technique. Corrections to the reflected intensity are more complex because part of the harmonic content is removed by reflection from the sample. The reflectivity in second order is obtained by assuming, for example, that a measure of the reflectivity in the range E=700-800 eV, where second order is negligible in the incident beam, approximates the second-order reflectivity at E/2 = 350 - 400 eV. Similar arguments can be made for third order harmonics. After correcting for harmonic contamination, the reflected intensity, I, is divided by the monitor intensity, I_o, to remove the effects of fluctuations in the incident beam intensity. Finally, geometric corrections are made for the spectrum length and the beam size.

For each sample, reflEXAFS data were accumulated for a minimum of five angles between $\phi = 0.5°$ and 3.5°. One method for deriving δ and β as a function of incident photon energy is to fit each set of reflectivity spectra. Alternatively, we used pairs of reflectivity spectra to solve directly for the two optical constants. The energy dependence of the absorption coefficient, μ, was obtained directly from the spectra for β. From this point on, the analysis followed standard EXAFS practice.

REFERENCES

A1. G.G. Long and J. Kruger, in "Techniques for Characterization of Electrodes and Electrochemical Processes," edited by R. Varma and J.R. Selman (Wiley, New York, in press).

A2. G. Martens and P. Rabe, Phys. Stat. Sol. (a) 58, 415 (1980).